Geophysical Journal International

Geophys. J. Int. (2015) **201,** 1156–1181 doi: 10.1093/gji/ggv066
GJI Geodynamics and tectonics

Glacial isostatic adjustment, relative sea level history and mantle viscosity: reconciling relative sea level model predictions for the U.S. East coast with geological constraints

Keven Roy and W.R. Peltier

Department of Physics, University of Toronto, Toronto, ON, Canada M5S 1A7. E-mail: kroy@atmosp.physics.utoronto.ca

Accepted 2015 February 9. Received 2015 February 6; in original form 2014 July 2

SUMMARY

Models of the glacial isostatic adjustment process, which is dominated by the influence of the Late Pleistocene cycle of glaciation and deglaciation, depend on two fundamental inputs: a history of ice-sheet loading and a model of the radial variation of mantle viscosity. These models may be tested and refined by comparing their local predictions of relative sea level history to geological inferences based upon appropriate sea level indicators. The U.S. Atlantic coast is a region of particular interest in this regard, due to the fact that data from the length of this coast provides a transect of the forebulge associated with the former Laurentide ice sheet. High-quality relative sea level histories from this region are employed herein to explore the ability of current models of mantle viscosity to explain the inferred evolution of relative sea level that have accompanied forebulge collapse following deglaciation. Existing misfits are characterized, and alternatives are explored for their reconciliation. It is demonstrated that a new model of mantle viscosity, referred to herein as VM6, when coupled with the latest model of deglaciation history ICE-6G_C, is able to eliminate the majority of these misfits, while continuing to reconcile a wide range of other important geophysical observables, as well as additional relative sea level data from the North American. West coast which also record the collapse of the forebulge but which have not been employed in tuning the viscosity profile to enable ICE-6G_C (VM6) to fit the East coast data set.

Key words: Sea level change; Transient deformation; Rheology: crust and lithosphere; Rheology: mantle; North America.

1 INTRODUCTION

The study of the glacial isostatic adjustment (GIA) process, through which the solid Earth responds viscoelastically to varying ice and water loads at its surface associated with the Late Quaternary ice-age cycle, has significantly contributed to our understanding of both palaeoclimatological phenomenology and solid Earth geophysics. A contribution in the latter area has involved the provision of robust constraints on the effective viscosity of the planetary mantle, a crucial ingredient in the design of models of the mantle convection process. Furthermore, comparisons of the relative sea level histories predicted by GIA models to the large and globally distributed database of geologically derived records of such histories, such as that originally assembled at the University of Toronto and described in Tushingham & Peltier (1992), has led to significant advances in our understanding of the most recent cycle of Late Quaternary glaciation and deglaciation. Knowledge of the geographical distribution and temporal variability of land ice over the approximately 100 000 yr period of this cycle provides the detailed boundary conditions of palaeotopography and palaeobathymetry that are required as a basis for the reconstruction of ice-age climate conditions using modern coupled atmosphere–ocean climate models (e.g. Peltier 1994, 2004; Vettoretti & Peltier 2013; Peltier & Vettoretti 2014). Because the quality of the relative sea level (RSL) database is especially high in the period since the Last Glacial Maximum (LGM) between 21 000 and 26 000 years ago (Peltier & Fairbanks 2006), the focus upon this period, both geophysically and climatologically, has been especially intense. This has led to the development of regional RSL databases with exceptional quality control such as that for the United Kingdom (Shennan *et al.* 2002), for the Canadian land mass that was once covered by the vast Laurentide/Cordilleran/Innuitian ice sheet complex (Dyke *et al.* 2002; Dyke 2004), and for both the East coast (Engelhart *et al.* 2011) and the West coast (Engelhart *et al.* 2014) of Canada and of the continental United States. The latter regions will be of special interest for the purpose of the present paper.

It is also important to appreciate the role played by the GIA-derived results concerning the last deglaciation event of the current ice age in the context of analyses of the renewed episode of continental deglaciation that is occurring due to the rapidly increasing

concentrations of atmospheric greenhouse gases. Our observations of the ongoing melting of both the great polar ice sheets on Antarctica and Greenland as well as small ice sheets and glaciers, which is responsible for an important fraction of the global rise of sea level occurring at the present time, is significantly impacted by the remaining isostatic disequilibrium associated with the last ice-age cycle, the signal of which must be eliminated in order to more clearly identify the global warming component (e.g. Peltier & Tushingham 1989; Peltier 2009). In particular, the GIA correction is central to the analysis of the time dependent gravity results being provided by the Gravity Recovery and Climate Experiment (GRACE) satellites and the determination of the recent melting of Greenland, Antarctica, and of other smaller ice catchments such as the Alaskan glaciers (e.g. Peltier 2009; Peltier & Luthcke 2009; Luthcke *et al.* 2013; Velicogna & Wahr 2013). Given the large potential economic and social impacts of future sea level changes, and as estimates of such melting vary wildly depending on the ice sheet loading history and GIA correction used (e.g. Ivins *et al.* 2013; Argus *et al.* 2014), it becomes crucial to evaluate models of the GIA process against all available geophysical observables and to consider them from a global perspective.

In this context, the Atlantic coast of the continental United States is a region of special interest for the study of the GIA process, given that data from this coast provides a transect of RSL history associated with the collapse of the forebulge induced outboard of the former Laurentide ice sheet that once covered all of the Canadian landmass to the north. Given the availability of a newly compiled database of ^{14}C-dated records of sea level evolution of very high quality for the Holocene period (Engelhart *et al.* 2011), it has become possible to more stringently test the accuracy of a recently constructed GIA model than had previously been possible given the modest quality control to which previous such compilations were subject. This is a primary goal of the present paper. We will fix the global ice sheet loading history to that of the most recently constructed model referred to as ICE-6G_C, which has been developed to eliminate the misfits to geodetic data identified in Argus & Peltier (2010) and Argus *et al.* (2014), and then proceed to identify any misfits of the predictions of the GIA model to the RSL histories tabulated in the Engelhart *et al.* (2011) database. We will initially fix the radial profile of mantle viscosity to the VM5a profile of Peltier & Drummond (2008) or to the variant upon it labelled VM5b in Engelhart *et al.* (2011). Our analyses of the misfits of the predictions of models ICE-6G_C (VM5a) and ICE-6G_C (VM5b) to the data of Engelhart *et al.* (2011) will lead us to a further refined model of mantle viscosity that we will refer to as VM6. However, it will be important to describe the systematic series of sensitivity analyses that have led us to this refined model. This will involve a search through the space of plausible parametrizations of viscosity depth dependence that will in many ways be ad hoc rather than based upon the application of the formal Bayesian methodology that led to the original VM2 model of Peltier (1996a, 1998a,b). The reason we have decided to follow this approach is that there does not appear to be an equally simple parametrization of the RSL histories from the forebulge region as that possible for histories from the regions previously covered by thick accumulations of land ice, where sea level histories have a simple exponential form described entirely by an amplitude and a characteristic relaxation time. Prior to implementing a brute force statistical search based upon Monte Carlo methods we will here pursue a restricted search during which we will be able to develop a physical understanding of the sensitivity of RSL histories from sites along the U.S. East coast to variations of viscosity over various depth intervals. The application of more formal methods will be discussed in later work.

2 THE GIA PROCESS: THEORETICAL BACKGROUND

The mathematical structure of the global GIA process was first developed in the 1970s in a series of seminal papers (Peltier 1974, 1976; Farrell & Clark 1976; Peltier & Andrews 1976; Clark *et al.* 1978; Peltier *et al.* 1978). It has since been extended and further refined from this earliest form. The current and most elaborate version of the theory, and the one that we will be employing herein, takes the form of a Fredholm equation of the second kind, an integral equation whose solution provides a prediction of the time varying level of the sea with respect to the continuously deforming surface of the solid Earth (e.g. Peltier *et al.* 2015). The explicit form of this sea level equation (SLE) is as follows:

$$S(\vartheta,\lambda,t) = C(\vartheta,\lambda,t)\Bigg[\int_{-\infty}^{t} \mathrm{d}t' \iint_{\Omega} \mathrm{d}\Omega' \left(G^{L}\left(\gamma, t-t'\right) L\left(\vartheta',\lambda',t'\right) + G_{R}^{T}\left(\gamma, t-t'\right) T\left(\vartheta',\lambda',t'\right)\right) + \frac{\Delta\Phi(t)}{g}\Bigg], \quad (1)$$

where $S(\vartheta,\lambda,t)$ represents the space and time varying local level of the sea relative to the continuously viscoelastically deforming local surface of the solid Earth at time t and at the geographical location with colatitude ϑ and longitude λ. The function $L(\vartheta',\lambda',t')$ is the surface mass loading history per unit area which consists of both grounded land ice and ocean water components. It may be written in the composite form:

$$L(\vartheta,\lambda,t) = \rho_I I(\vartheta,\lambda,t) + \rho_w S(\vartheta,\lambda,t). \quad (2)$$

In eq. (2) ρ_{I} and $I(\vartheta,\lambda,t)$ represent ice density and ice thickness history, whereas ρ_w and $S(\vartheta,\lambda,t)$, respectively represent water density and relative sea level. The integral nature of eq. (1) is thus clear on the basis of the fact that the unknown field 'S' appears both in the integrand of eq. (1) and on its left-hand side. The function $T(\vartheta',\lambda',t')$ represents the change in centrifugal potential forcing to which both the solid Earth and the oceans are subject due to the changing rotational state of the planet. These rotational changes are induced by the large mass movements associated with the glaciation and deglaciation processes. The solutions of the sea level equation to be employed herein include the renormalized representation of the rotational feedback terms discussed explicitly in Peltier *et al.* (2012).

In eq. (1) the functions $G^{\mathrm{L}}(\gamma, t-t')$ and $G^{\mathrm{T}}_{\mathrm{R}}(\gamma, t-t')$ are the Green functions which, when convolved with the surface mass and centrifugal potential loading terms, predict the evolving separation between the surface of the solid Earth and the surface of the sea. The angle γ represents the separation between the source point and the field point at which the response is to be determined. The exact formulation of the impulse function G^{L} was first described in Peltier (1974), subsequently refined in Peltier & Andrews (1976) and Peltier (1985), and takes the form:

$$G^{\mathrm{L}}(\gamma,t) = \frac{a}{M_{\mathrm{e}}} \sum_{l=0}^{\infty} \left[1 + k_{\mathrm{l}}^{\mathrm{L}}(t) - h_{\mathrm{l}}^{\mathrm{L}}(t)\right] P_{\mathrm{l}}(\cos\gamma). \quad (3)$$

In eq. (3), a and M_{e} refer to the Earth's mean radius and mass, while the $P_{\mathrm{l}}(\cos\gamma)$ are the standard Legendre polynomials evaluated at angle γ, and $k_{\mathrm{l}}^{\mathrm{L}}(t)$ and $G_{\mathrm{l}}^{\mathrm{L}}(t)$ are the time-dependent viscoelastic surface load Love numbers which constitute time dependent viscoelastic extensions of the equivalent elastic surface load Love numbers of Farrell (1972). A similar formulation exists for the Green function $G^{\mathrm{T}}_{\mathrm{R}}(\gamma, t)$ associated with the change in centrifugal

potential $T(\vartheta', \lambda', t')$, which includes corresponding time-dependent viscoelastic Love numbers $k_l^T(t)$ and $h_l^T(t)$. This form has been reviewed recently in Peltier *et al.* (2012).

The function $C(\vartheta, \lambda, t)$ in eq. (1) is the so-called *ocean function*, which has a value of unity over oceans and zero elsewhere. The time-dependent function $\Delta\Phi/g$ is constructed so as to ensure that there is a precise match between the mass of water generated by melting ice and that which appears in the ocean basins (see Peltier 1998c, 2002, for thorough discussions of this term). The complete sea level eq. (1) is solved in such a way as to simultaneously compute the time dependence of the ocean function using the iterative methodology introduced in Peltier (1994, 1998d) and Peltier & Fairbanks (2006).

The required inputs to eq. (1) consist of two geophysical fields, namely a global ice loading history $I(\vartheta, \lambda, t)$, and a spherically symmetric radial viscosity structure (on the basis of which the exact forms of the time-dependent viscoelastic Love numbers $k_l^L(t)$, $h_l^L(t)$, $k_l^T(t)$ and $h_l^T(t)$ are determined). Our attention turns next to these two important components of the theory.

3 THE ICE-NG MODELS OF ICE SHEET LOADING HISTORY

The first input required to infer a global evolution of relative sea level is a history of ice sheet loading associated with the last glaciation/deglaciation cycle. Such ice sheet history models are partly constrained on the basis of surface geomorphological evidence, such as carbon-datable material from terminal moraines which mark the margins of a land ice sheet in its retreat phase. In the recent past, cosmogenic exposure age dating, which may be invoked to determine the time since a surface outcrop or glacial erratic boulder has been exposed following the retreat of an ice sheet that once covered the location, has become a widely employed tool (e.g. Dyke *et al.* 2002; Dyke 2004; Whitehouse *et al.* 2012; Argus *et al.* 2014). These methods are particularly suited to infer the evolution of the margins of large concentrations of ice, but most often only weakly constrain the evolution of ice thickness. Significant progress in the estimation of the evolving thickness of ice was only realized through application of GIA analyses. Because of the simple exponential relaxation form of relative sea level records from regions that were previously covered by thick ice sheets (e.g. Canada, Fennoscandia), one may employ the amplitude of the exponential rebound curves to 'weigh' the thickness of the ice that must have been removed to induce the amplitude of the rebound observed. This requires, however, that the viscosity structure of the Earth's deep interior be known. As discussed in several of the available reviews of the theory that has been developed to perform such analyses (e.g. Peltier 1982, 1998c, 2007), it is possible to separate the problem of weighing the ice to determine its thickness from the problem of determining deep earth viscosity by obtaining the latter first on the basis of observations of the relaxation times characteristic of the RSL histories in previously glaciated regions. The amplitude of these rebound time series may then be employed to constrain ice thickness if additional constraints are available on the timing of load removal.

Early attempts to provide a history of ice sheet loading (e.g. Peltier & Andrews 1976; Wu & Peltier 1983) were greatly improved through the application of a large database of relative sea level histories spanning the whole globe. This set of *a posteriori* constraints led to the development of the ICE-3G structure, presented in Tushingham & Peltier (1991). Subsequent changes, which included refinements in the analysis methodology and the use of further observational constraints such as the high-quality Barbados RSL history based upon U-Th dating of coral terraces (Fairbanks 1989), resulted in the improved ICE-4G model (Peltier 1994). Later, the ICE-5G model (Peltier 2004) was refined using high-quality geodetic and gravity data, most notably over North America (Argus *et al.* 1999), and extended the ice loading history to the entirety of the most recent glacial–interglacial cycle. Other improvements to the model included the application of refined GIA data over the British Isles (Peltier *et al.* 2002; Shennan *et al.* 2002) and new observations of far-field sea level histories (Peltier 2004). The ICE-5G model has been widely used in conjunction with the VM2 viscosity profile of the mantle to provide a global theory of relative sea level adjustment due to the glaciation/deglaciation process.

Further refinements to the ICE-5G loading history over North America have more recently been introduced, in which the misfits to Global Positioning System (GPS) observations of vertical motion of the crust documented in Argus & Peltier (2010) have been eliminated by appropriate modifications of the ice thickness history over North America, Northwestern Eurasia and Antarctica. This process has led to the ICE-6G_C model (Argus *et al.* 2014; Peltier *et al.* 2015). Fig. 1 shows a comparison of the LGM topography of

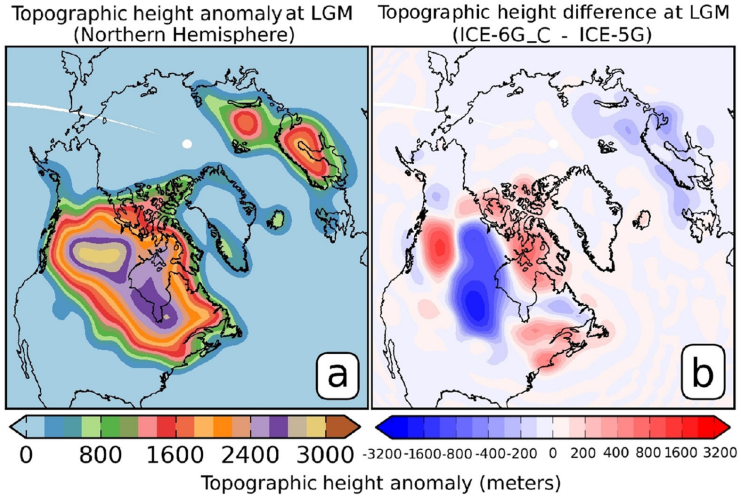

Figure 1. (a) Topographic height anomaly at LGM in the Northern hemisphere for the ICE-6G_C ice loading history. (b) Difference in topographic height at LGM between the ICE-6G_C loading history and its ICE-5G predecessor (Peltier 2004). Figure modified from Vettoretti & Peltier (2013).

this most recent model with respect to LGM sea level over North America with that of the precursor ICE-5G model. Inspection will show that the primary modifications of the ice thickness distribution consist of a thinning of the Laurentide ice sheet in central Canada and a thickening over northern Quebec and Labrador, as well as over the northern border region between the Canadian provinces of Alberta and British Columbia. The Antarctic component of the global model is discussed in Argus *et al.* (2014). This modified model, which is being referred to as ICE-6G_C, will be employed for the purpose of all of the analyses to be discussed in the present paper.

4 ANALYSIS OF THE PERFORMANCE OF THE ICE-6G_C ICE LOADING HISTORY AS A FUNCTION OF VISCOSITY MODEL

One of the primary observational data sets which enables the testing of models of the GIA process consists of reconstructions of past sea level evolution, which can be derived from the isotopic dating (^{14}C or U-Th) of relevant biological markers interpreted in the context of their possible elevation range with respect to relative sea level at the time of their growth (e.g. van de Plassche 1986). Examples of such indicators include shells of intertidal or marine mollusc species (providing a sea level range or a marine limit, respectively), high/low marsh plants and salt marsh microfossils indicating a freshwater limit, or coral samples that indicate a possible range of relative sea level based on the depth range of the specific species studied. Today, an extensive number of such records exist at a wide range of locations around the globe, and they provide invaluable constraints on the evolution of relative sea level, most notably at locations that are key to the study of the GIA process. Among these regions for which especially high quality records now exist, the eastern seaboard of the United States is of particular interest. As mentioned in the previous sections, this is because it straddles the glacial forebulge which consists of an upwarping of the crust of the solid Earth that was induced by the viscous flow of material from the Earth's interior beneath the previously ice sheet covered region into its periphery. This forebulge region extends from slightly south of the LGM margin of Laurentian ice southwards into the Caribbean Sea. Its trailing edge is located in the near vicinity of the critical island of Barbados.

4.1 The Engelhart *et al.* (2011) data set of RSL evolution along the U.S. East coast

One of the key prerequisites for the analysis of the geographical patterns of relative sea level evolution on the East coast of the United States is the availability of an adequate observational data set. In this analysis, the quality-controlled database presented by Engelhart *et al.* (2011), a data set consisting of 686 individual sea level indicators from locations along the coast ranging from northern Maine to South Carolina, will be employed. These data may be assigned to 16 distinct locations, which are indicated on Fig. 2(a).

A substantial advantage of this particular data set, which constitutes a significant improvement over that employed in Tushingham & Peltier (1992) or Peltier (1996b) for the same region, derives from the fact that the methodology employed for its construction has been highly systematic and significant efforts have been invested in assigning meaningful error estimates to each of the sea level indicators employed (Engelhart *et al.* 2011).

4.2 Analysis of the performance of the VM5a and VM5b viscosity structures

The study of the geophysical observables associated with the GIA process provides information about the viscosity structure of the solid Earth. Early models of the radial structure of the viscosity of the mantle, such as the VM1 model, were simple two-layer models that attempted to distinguish the viscosity between the average values appropriate for the upper and lower mantle with the boundary between these regions defined by the phase transition interface at 660 km depth (Peltier *et al.* 1986; Tushingham & Peltier 1992). Using a theoretical framework based on the formal Bayesian methodology (Mitrovica & Peltier 1991, 1993; Mitrovica & Peltier 1995), various observables were considered in an effort to better understand their resolving power for the inference of viscosity depth dependence. Thereafter, Peltier (1996a) used the totality of the data, each type having its own resolving power insofar as viscosity depth dependence is concerned, to demonstrate that when all such data were employed one could obtain estimates of mantle viscosity from the surface to the core–mantle boundary. These data included the Fennoscandian relaxation spectrum of relaxation times (described below), a suite of site-specific relaxation times in regions heavily influenced by the former Laurentide and Fennoscandian ice sheets, as well as two anomalies of the Earth's rotational state: the speed and direction of the true polar wander phenomenon and the rate of non-tidal acceleration of the Earth's axial rotation rate (Peltier & Jiang 1996). The resulting profile of radial variations in viscosity, referred to in the literature as VM2, is presented in Fig. 3(a) where it is shown to be capped by a 90-km elastic lithosphere. Despite the high-quality fits that the VM2 viscosity profile combined to the ICE-5G history of ice sheet loading provided when compared to a large number of globally distributed ^{14}C-dated relative sea level histories (Peltier 2004), discrepancies were subsequently found to exist between predicted and observed modern-day horizontal motion of the crust of the solid Earth over North America (Argus *et al.* 1999; Sella *et al.* 2007). These results were obtained from an extensive network of GPS observations over the continent. Peltier & Drummond (2008) demonstrated that the horizontal velocity misfits could be eliminated by a simple modification of the shallow structure that was characteristic of the VM2 viscosity profile by introducing radial viscosity stratification of the near-surface lithosphere, a feature that is expected based on the exponential temperature dependence of the creep resistance of a solid. Their preferred viscosity profile, referred to as VM5a, is a 5-layer approximation to the VM2 viscosity profile which incorporates a 60-km elastic lithosphere overlaying a 40-km region of high viscosity (10^{22} Pa s), which then becomes at greater depths a multilayer average of the VM2 model (Peltier & Drummond 2008).

Engelhart *et al.* (2011) compared predictions of relative sea level history at locations along the U.S. East coast for the VM5a viscosity structure when combined with either the ICE-5G or an early version of the ICE-6G ice loading history with their observational database and found persistent misfits between them, irrespective of which of these loading histories was employed. In an initial simple attempt to eliminate these misfits, they introduced the VM5b viscosity profile, a modified version of the VM5a profile for which the viscosity was halved in the upper mantle and transition zone. Such a modification was found to remove some of the identified discrepancies in the

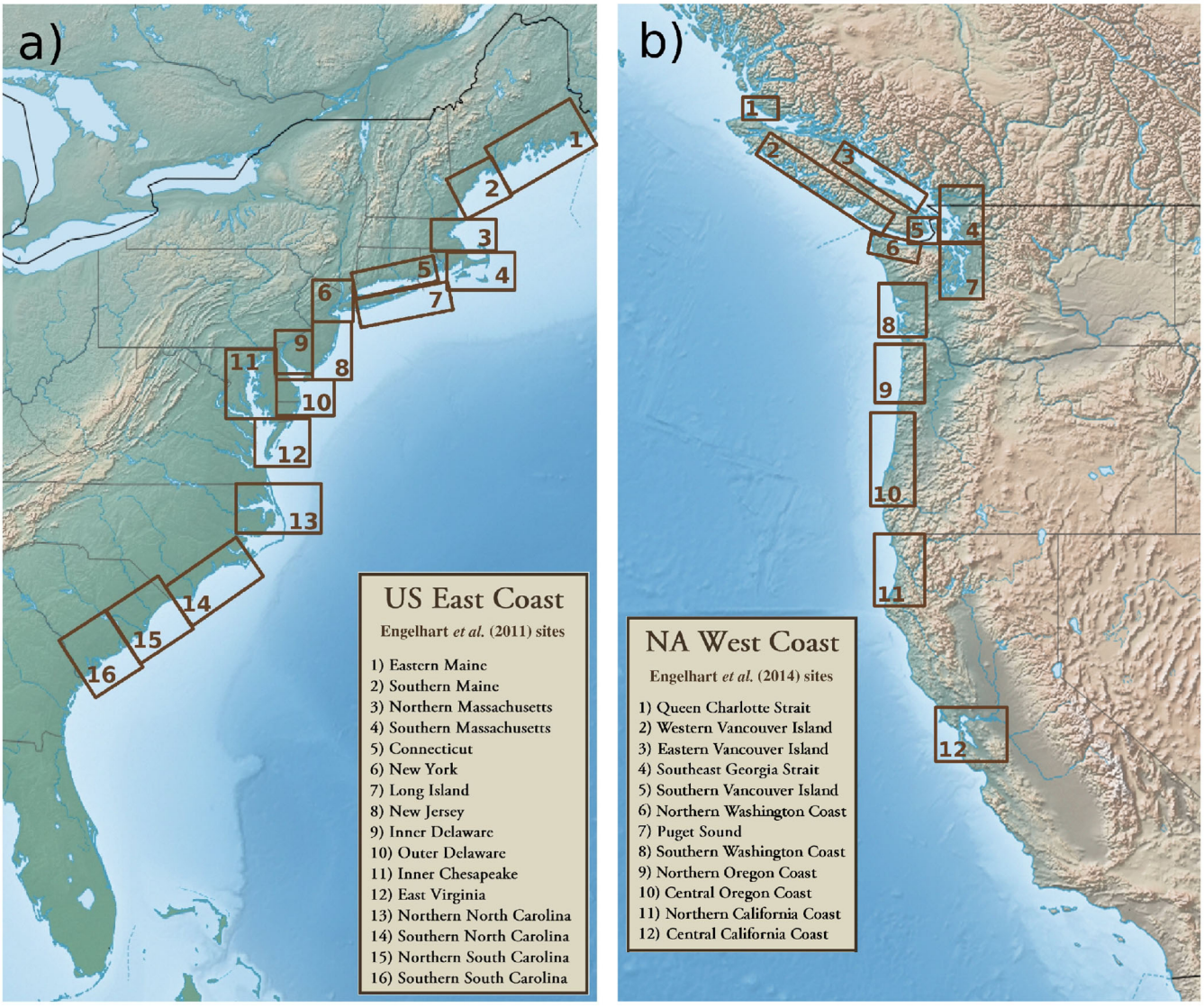

Figure 2. (a) Geographical location of the 16 composite sites identified in Engelhart *et al.* (2011) along the U.S. East coast and used in the current work. (b) Geographical extent of the 12 composite sites used in the current work for the North American West coast (Engelhart *et al.* 2014).

mid-Atlantic region, although significant misfits remained for the southernmost part of the region covered by the data set. The VM5a and VM5b profiles are presented in Fig. 3(a), together with the parent VM2 profile.

We begin our analyses by revisiting the model predictions of relative sea level histories based upon the use of the VM5a and VM5b viscosity profiles and of the ICE-6G_C ice loading history, compared to the Engelhart *et al.* (2011) data set, using the most recent version of the University of Toronto model. All model predictions include the impact of rotational feedback. The resulting comparisons are shown in Fig. 4 for the 16 distinct locations for which data is included in the compilation.

For the northernmost locations (Southern Maine, MA), inspection of the fits to the observational data shows that the VM5a profile performs better than VM5b, as the softer model of the upper mantle and transition zone predicts the existence of a high stand, which is not observed in the observational records, and significantly underpredicts relative sea level changes over the past few millenia. It is worthwhile to note that for Eastern Maine, neither VM5a nor VM5b succeeds in reconciling model predictions and observations. In fact, the predictions of the two models bracket the observations. Progressing further south along the coast, the performance of the VM5a model degrades noticeably, while the VM5b model is either the equal of VM5a or an improvement, depending on the region of interest. For coastal Connecticut and New York, neither of the models adequately reproduces the observed relative sea level evolution, but they rather bracket the observations. Continuing further south, the VM5b profile begins to perform better than VM5a for coastal locations (in Long Island, New Jersey, Outer Delaware and East Virginia), although misfits remain for observations older than 6.5 ka. VM5a and VM5b bracket the available observations for the regions further inland (Inner Delaware, Inner Chesapeake). However, progressing into North Carolina, the misfits between the observations and the model predictions for both VM5a and VM5b become larger for the earliest part of the records. Model predictions become very similar for both VM5a and VM5b, and a clear misfit can be identified prior to 5 ka for the locations in North Carolina and South Carolina. Thus, although the VM5b profile does indeed provide an improvement in performance for mid-Atlantic locations (Engelhart *et al.* 2011), both models remain unacceptable for the southernmost sites.

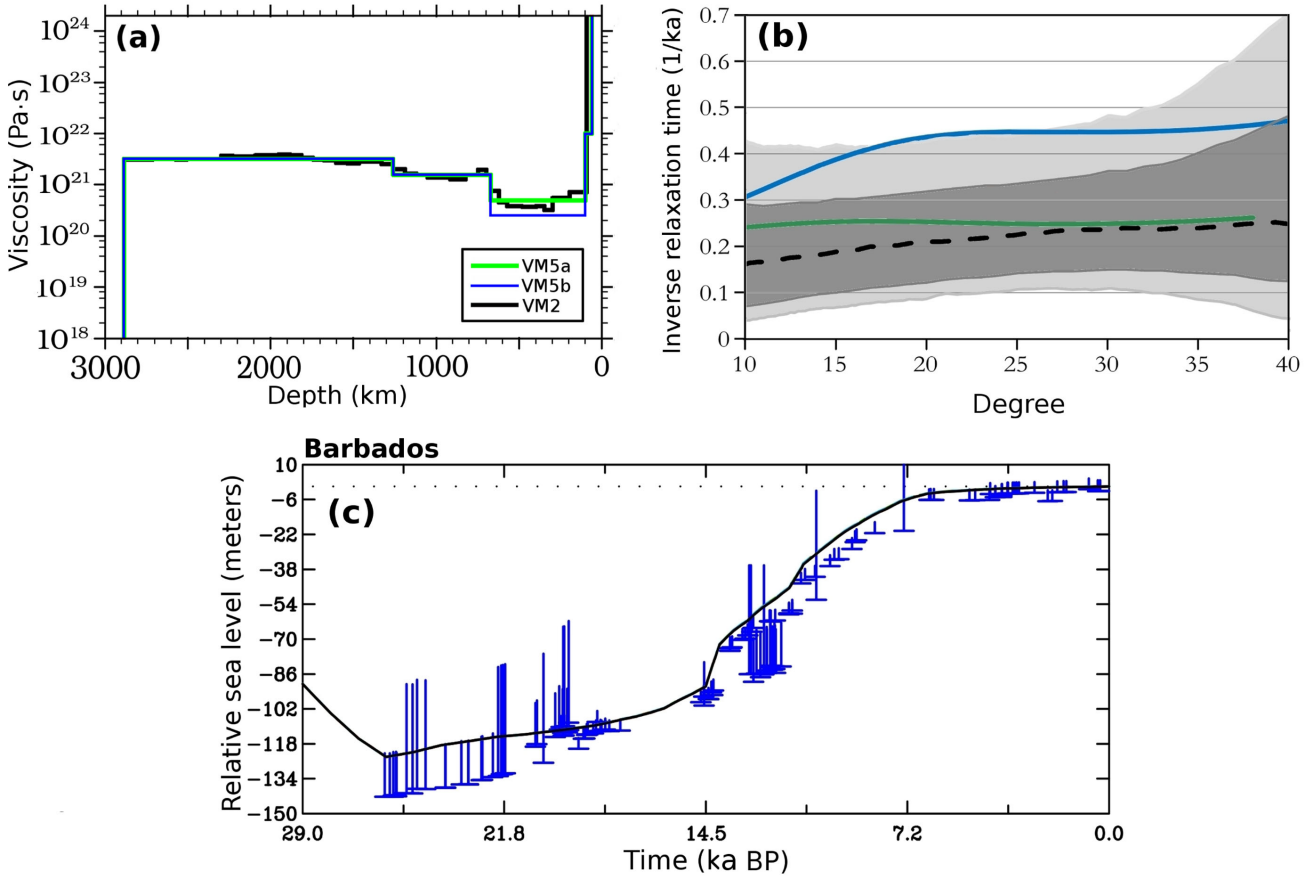

Figure 3. (a) Radial variations of the viscosity in depth for the viscosity profiles VM5a (green), VM5b (blue) (note that VM5a and VM5b are identical except in the upper mantle), and VM2 (black), for which VM5a is a 5-layer approximation with added stratification (high viscosity layer between 60 and 100 km depths) just below the elastic lithosphere (0–60 km depth). (b) Inverse relaxation time as a function of spherical harmonic degree obtained from observations of the glacial isostatic adjustment of Fennoscandia, with the relaxation spectrum (black dashed line) and corresponding 1σ uncertainties (dark grey area) calculated by Wieczerkowski *et al.* (1999), with the inferred 2σ uncertainties extending to the light grey area. The predicted spectra for the VM5a model (green) and for the VM5b model (blue) are superimposed. (c) Fit of the ICE-6G_C model predictions to the Barbados record of coral-based sea level indicators when combined to the VM5a viscosity structure.

4.3 The fit to the Fennoscandian spectrum

An important caveat needs to be addressed concerning the marginal increase in performance of the VM5b viscosity profile, which concerns its fit to one of the most important observational data sets relating to the GIA process, namely the fit to the so-called Fennoscandian spectrum of relaxation times, first derived by McConnell (1968).

Fennoscandia is a region of considerable interest with regards to the study of the GIA process, due to the large ongoing surface adjustments due to the influence of the former ice sheet which covered it during the last glaciation-deglaciation cycle (e.g. Steffen & Wu 2011). The Fennoscandian spectrum provides, as a function of deformation wavelength, a series of constraints on the relaxation time associated with the GIA process, which have been inferred using a database of six former strandlines from different locations along the coast of the Gulf of Bothnia and of the Gulf of Finland. The analysis of McConnell (1968) has been shown to provide a constraint on Earth rheology to a depth of approximately 1500 km, with the considerable advantage of being relatively insensitive to the temporal and geographical evolution of the thickness of the Fennoscandian ice sheet. This important property has led to considerable interest being devoted to the area and to the data set employed (e.g. Mitrovica & Peltier 1993; Peltier 1998c; Wieczerkowski *et al.* 1999; Steffen & Wu 2011). In particular, Wieczerkowski *et al.* (1999) applied a damped least-squares solution methodology to the strandline data of Donner (1995) to revisit the McConnell (1968) constraints. Their result provided a somewhat modified inference of the relaxation time dependence on deformation wavelength, complete with a 1σ uncertainty range, which is reproduced in Fig. 3(b) with an uncertainty extended to 2σ, together with the prediction of the spectrum for the VM5a and VM5b viscosity profiles.

While the VM5a profile succeeds in producing a relaxation time spectrum consistent with the inferences of McConnell (1968) and Wieczerkowski *et al.* (1999) (unsurprisingly so, as it is a 5-layer approximation to the VM2 profile, which is heavily constrained by the spectrum (Peltier 1996a)), the VM5b profile fails to reproduce the Fennoscandian spectrum, especially at longer wavelengths (lower spherical harmonic degree). The inability of the VM5b model to reproduce this crucial constraint strongly indicates that the gain in performance from the VM5b profile in the mid-Atlantic is illusory as accepting it would require one to entertain models with significant lateral heterogeneity of viscosity and our goal in the first instance is to attempt to define the best possible spherically symmetric model of the Earth's viscosity structure.

The focus of the further analyses to follow is therefore to attempt to optimally reconcile observations of relative sea level evolution on the U.S. East coast with predictions of a spherically

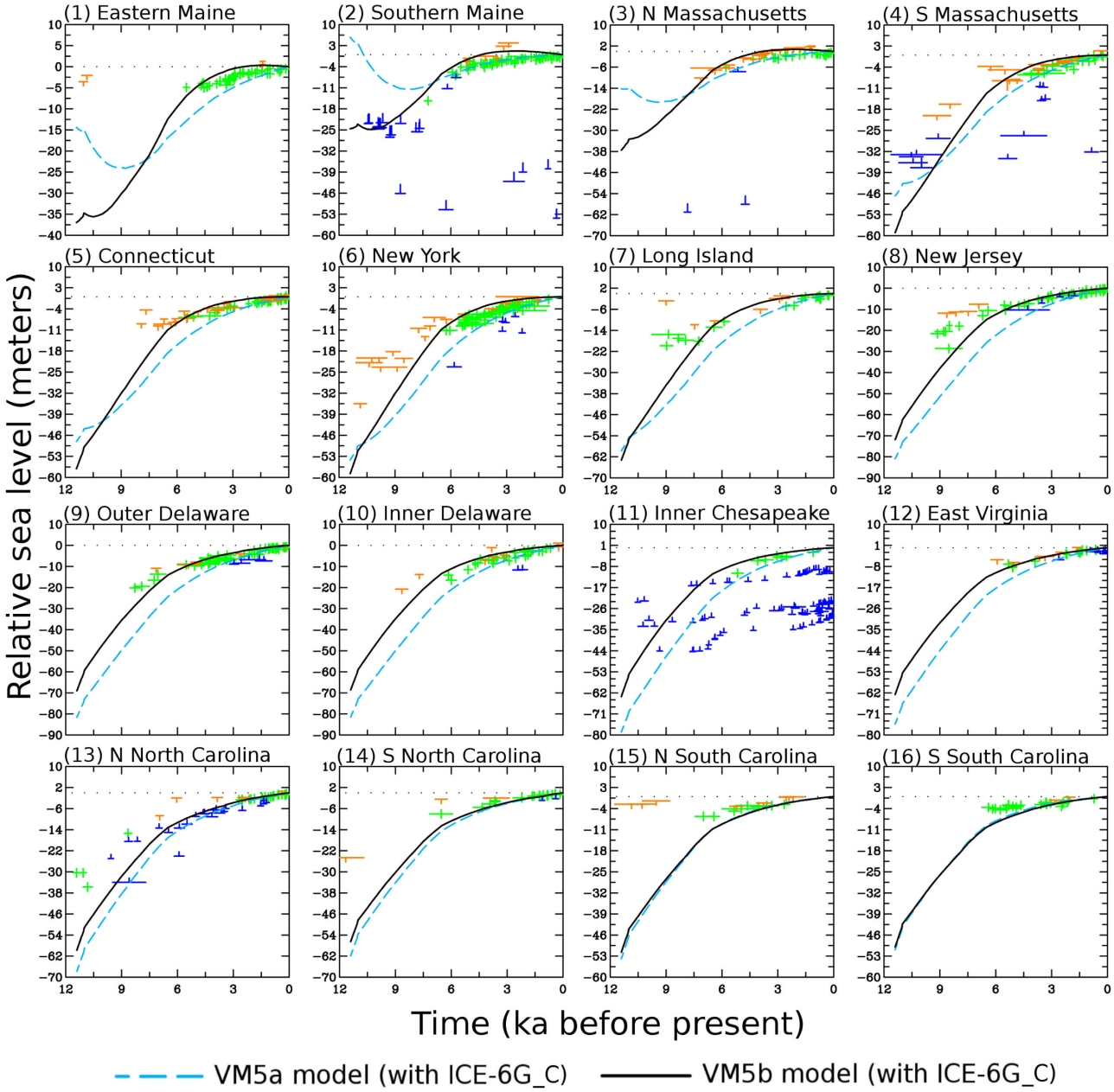

Figure 4. Comparison of the Engelhart *et al.* (2011) data set of relative sea level histories along the U.S. Atlantic coast for the 16 composite regions with the predicted relative sea level history at those locations for the ICE-6G_C model of ice-loading history combined to the VM5a (blue) and VM5b (black) radial viscosity profiles. Green data points represent sea level index points, whereas blue crosses represent marine-limiting data and orange crosses represent terrestrial-limiting data.

symmetric model, while maintaining an acceptable fit to other key constraints related to the GIA process, including that provided by the Fennoscandian relaxation spectrum.

5 AN EXPLORATION OF ALTERNATIVE VISCOSITY STRUCTURES

The nature of the misfits identified between observational data and model predictions of relative sea level evolution on the U.S. East coast is investigated in what follows. We will attempt to eliminate these misfits using suitable variations of the radial mantle viscosity structure, while maintaining a good fit to other geophysical constraints, such as the Fennoscandian spectrum of relaxation times.

5.1 Basic assumptions and methodology employed

In this analysis, we will employ a two-pronged approach, in which we will first explore the reasonableness of some alternative viscosity structures that have been suggested in the literature, and which differ significantly from the VM2/VM5a profiles. In particular, we will focus on the V1 and V2 structures, based on the work of Forte & Mitrovica (1996). Following this initial analysis, and having demonstrated that these alternatives are not in fact acceptable substitutes for the Toronto models, our second step will be to perform a direct analysis of the sensitivity of model predictions of sea level evolution on U.S. East coast to radial viscosity variations at different depths. As described earlier, all analyses for which results will be presented are performed using the ICE-6G_C ice loading history (Argus *et al.*

2014; Peltier *et al.* 2015), since it is a self-consistent global model constrained, among other observables, by the total eustatic sea level change that has occurred since the LGM at the far-field Barbados location (Peltier & Fairbanks 2006). The fit provided by the model is illustrated in Fig. 3(c) when used in conjunction with the VM5a viscosity structure. Our final step will be to combine the implications of all of the sensitivity analyses into a single model of radial viscosity structure, which we will call VM6. The high quality of the fit of this model to the totality of the geophysical observables will then be demonstrated, including not only the Fennoscandian spectrum of relaxation times and the relative sea level evolution along the U.S. East coast to which the model is tuned, but also independent tests that include a comparison to relative sea level evolution data along the U.S. West coast and the overall shape of the late Holocene forebulge along the Atlantic coast.

In this analysis, it is important to note that we will be focusing solely on spherically symmetric models of mantle viscosity. Even though lateral heterogeneity in mantle viscosity is fully expected to exist based on our knowledge of the temperature dependence of the creep resistance of mantle material, our goal is to develop a model of minimal complexity. We therefore see it as important to explain as many geophysical observables as possible using a simple spherically symmetric model, as this is intended to provide a suitable background viscosity structure onto which accurately inferred lateral viscosity variations may be superimposed.

As mentioned before, in our methodology, the ice model is fixed in all cases explored to ICE-6G_C. However, as models of the GIA process have as inputs both the viscosity structure of the planet's interior and a suitable history of ice sheet and ocean loading on its surface, it should be noted that this work is thus part of an iterative process during which these two input fields should be allowed to vary in turn. The goal of such an approach is to reduce the overall misfit between GIA model predictions and all available relevant geophysical observables, using the knowledge that the misfits to different observables are sensitive to different model inputs in order to eventually reach convergence. This work focuses solely on the impact of the viscosity structure on these misfits, while follow-up work will focus on the ice loading history and will enable us to address in a more definitive manner the issue of non-uniqueness.

5.2 Error analysis and model performance

The performance of the viscosity structure variations considered in this study is first determined by a visual inspection of the difference in relative sea level evolution at all locations along the U.S. East coast, which provides an invaluable source of information about the complex variations in the temporal and geographical responses of the forebulge. This analysis is complemented by a quantitative analysis of the misfit between the relative sea level index and limiting data points and the model predictions, which is described by a χ^2 relationship defined as:

$$\chi^2 = \frac{1}{N}\sum_{i=1}^{N}\left(\frac{\Delta_i}{\sigma_i}\right)^2. \tag{4}$$

In this relationship, N represents the number of historical data points (index points and limiting data points) and σ_i is the uncertainty in the sea level height of the ith data point (95 per cent confidence level). Also, Δ_i represents the difference between an observed sea level indicator and the model prediction. For sea level index points, it takes the form:

$$\Delta_i = S_i^{\text{obs}} - S_i^{\text{pred}}, \tag{5}$$

where S_i^{obs} represents the observed sea level height and S_i^{pred} is the model prediction. As they provide an upper or lower restriction on relative sea level, limiting data points should only have a non-zero contribution to the χ^2 function if the predicted sea level falls above a terrestrial-limiting data height or below a marine-limiting height. In the terrestrial-limiting case, the expression for the difference Δ_i is written as:

$$\Delta_i = \begin{cases} S_i^{\text{pred}} - h_i^{\text{obs}} + \sigma_i & \text{if } S_i^{\text{pred}} \geq (h_i^{\text{obs}} - \sigma_i) \\ 0 & \text{otherwise} \end{cases}, \tag{6}$$

where h_i^{obs} is the height of the observed limiting observational data point. In the case of a marine-limiting data point, Δ_i takes the form:

$$\Delta_i = \begin{cases} h_i^{\text{obs}} - S_i^{\text{pred}} + \sigma_i & \text{if } S_i^{\text{pred}} \geq (h_i^{\text{obs}} - \sigma_i) \\ 0 & \text{otherwise} \end{cases}. \tag{7}$$

The uncertainty in the age of the observational data points is taken into account in a simple manner: if the predicted sea level falls below the 95 per cent confidence height interval of an observation, the difference Δ_i is calculated for the time at the upper edge of the age uncertainty range, while it is calculated at the lower edge of the age uncertainty range if the predicted sea level is above the 95 per cent confidence height interval of an observation.

In all cases, the χ^2 values are defined for each site along the U.S. East coast as well as for the entire coast and a subensemble of the four southernmost locations, in order to focus specifically on the regional model response to depth-dependent mantle viscosity perturbations.

5.3 Alternative viscosity models: V1 (FM) and V2 (FM)

An alternative family of viscosity models under consideration in this study is derived from a methodology that involved a joint inversion of data that are related both to the mantle convection process and to GIA (Forte & Mitrovica 1996, 1997; Mitrovica & Forte 2004). The convection data sets used in those two studies include a map of the free-air gravity field, the non-hydrostatic ellipticity of the core–mantle boundary from measurements of the Earth's free-core nutation, the horizontal divergence of tectonic plates (e.g. Forte *et al.* 1991) and a map of dynamic topography (Forte *et al.* 1993; see also Pari & Peltier 1996, 2000), while the GIA data includes postglacial relaxation times for the Fennoscandian region and for Hudson Bay (two separate locations in James Bay and at Richmond Gulf, which turns out to be problematic, as will be discussed later). Their analysis was performed using a non-linear, iterative, Occam-style procedure, and was further refined in the upper mantle using site-specific decay times (Forte & Mitrovica 1996; Mitrovica & Forte 2004). A soft layer was included in the analysis just above the 660 km discontinuity, as had been earlier introduced in the papers of Forte *et al.* (1991) and Pari & Peltier (1995), who had argued for its existence as a consequence of transformational superplasticity due to grain size reduction during the transformations of mineral phase that would have occurred as material flows across the transition interface as a consequence of mantle convection. The resulting preferred model of Mitrovica & Forte (2004), referenced herein as V1 (FM), is presented in Fig. 5. The second model shown in the same figure, referenced herein

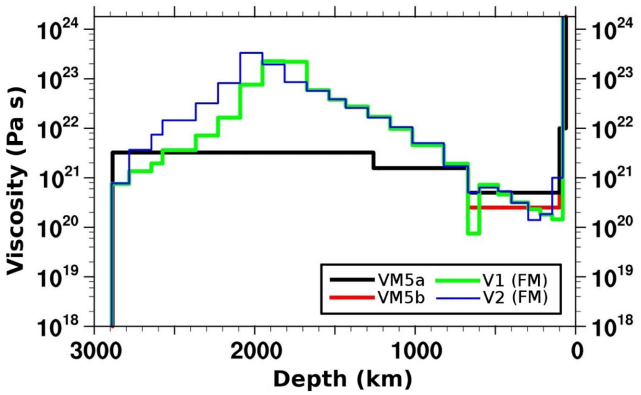

Figure 5. Comparison of the viscosity profiles VM5a (black) and VM5b (red) with the V1 (FM) profile of Mitrovica & Forte (2004) (green) and the V2 (FM) variation profile of Forte *et al.* (2009) (blue).

as V2 (FM), was presented in Moucha *et al.* (2008) and Forte *et al.* (2009), and is a variation based upon the same methodology, but where the thin low-viscosity layer is practically absent and where the lower mantle is more viscous.

The relative sea level history predictions for these two viscosity structures when combined with the ICE-6G_C ice loading history are shown in Fig. 6, where they are compared to the Engelhart *et al.* (2011) data set for a subset of four locations (Southern Maine, New York, Inner Delaware and Southern South Carolina). The comparison of the predictions resulting from these two viscosity structures for the other locations that make up the data set is provided in the Supplementary Materials section (Fig. S1). For the northernmost part of the Atlantic coast of the United States, the two FM profiles display predictions that are very similar to those of VM5a. However, for locations further south along the East coast, into regions located within the remains of the proglacial forebulge associated with the maximal extent of the former Laurentide Ice Sheet, the two FM profiles become less and less able to explain the geological data, with a systematic decrease of the quality of the fit as a function of latitude,

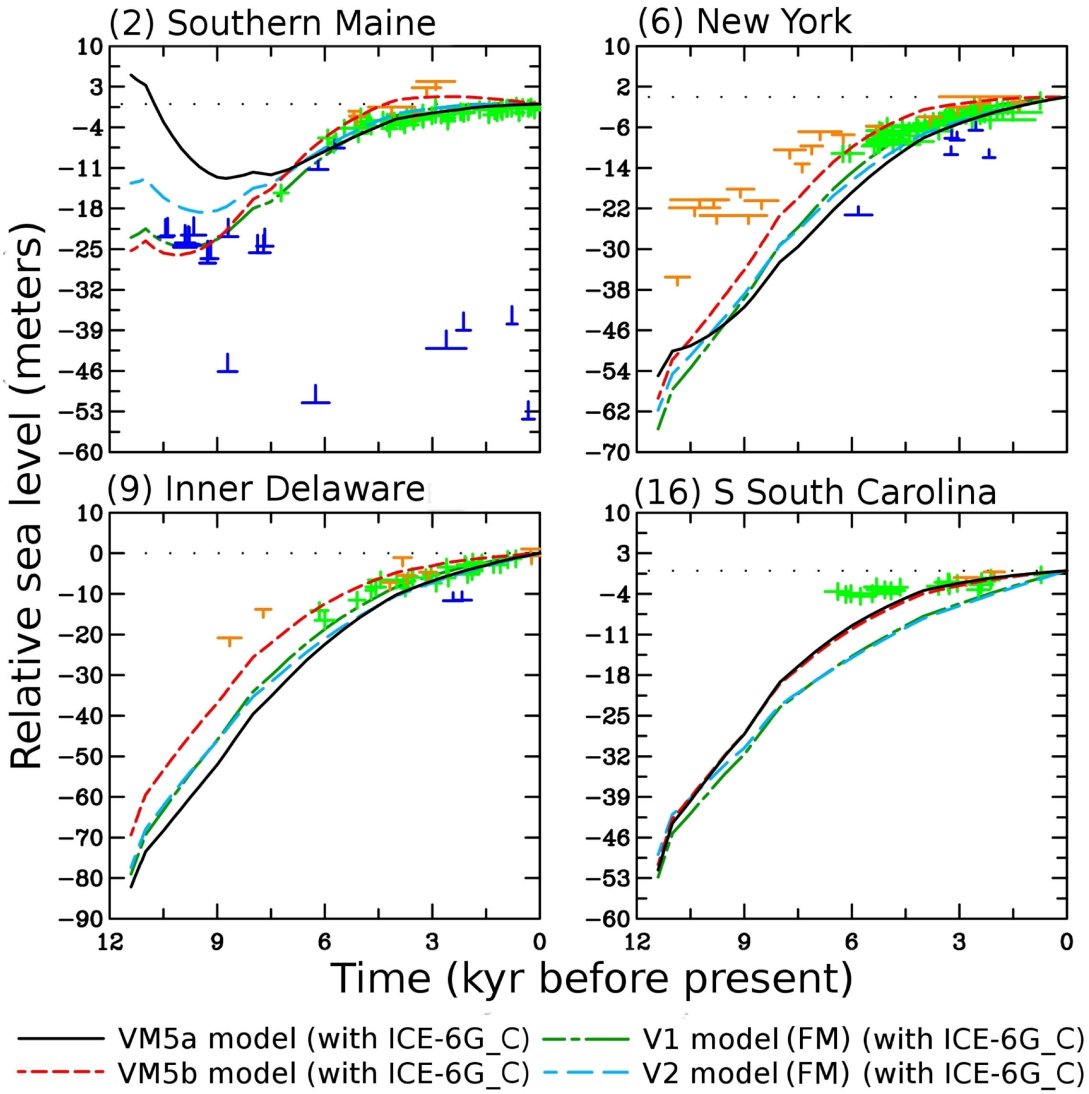

Figure 6. Comparison of a subset of regions of the Engelhart *et al.* (2011) data set of relative sea level histories along the U.S. Atlantic coast with the predicted relative sea level history at those locations for the ICE-6G_C model of ice-loading history combined to the V1 (green) and V2 (blue) radial viscosity profiles. Green data points represent sea level index points, whereas blue crosses represent marine-limiting data and orange crosses represent terrestrial-limiting data.

which becomes particularly acute in the Carolinas. In particular, in South Carolina, the misfit characterizing the use of the VM5a and VM5b profiles with ICE-6G_C is notably worsened by a switch to the alternative FM models (V1 and V2). This could be explained by their overall higher viscosity in the lower mantle, which would tend to further extend the region of proglacial forebulge collapse associated with deglaciation following the LGM.

One possible limitation of this comparison might come from the fact the ICE-6G_C ice loading history is optimized for the VM5a model, and might thus be expected to fail when combined with another viscosity structure, especially if very different from the VM5a model. One way to explore this possibility is to consider predictions that do not depend significantly on the ice loading history, such as the relaxation time experienced by the solid Earth under formerly heavily glaciated areas like Hudson Bay (at the centre of the former Laurentide Ice Sheet) or Fennoscandia. As these regions were under considerable ice cover at LGM, model-predicted relaxation times at locations near the centre of the ice loads are relatively protected from load history uncertainties near the ice sheet margins. For the Hudson Bay area, analyses performed by Peltier (1998c) on a complete set of ^{14}C-dated RSL constraints suggested a best estimate for the relaxation time in Hudson Bay (Richmond Gulf, Québec) of approximately 3.4 ka, whereas the ICE-4G (VM2) model predictions suggested a relaxation time of approximately 4.1 ka. A subsequent analysis of this data set by Mitrovica *et al.* (2000) led them to revisit the Peltier (1998c) inference, on the premise that close sites in the area might have largely different relaxation times which would be reflected on the individual curves for each site and that only a single type of RSL data should be employed. They suggested that the relaxation time at the Richmond Gulf site is approximately 5.0 ka (with a permissible range of 4.0–6.6 ka) and that it should be significantly lower at James Bay, at around 2.5 ka (with a permissible range of 2.0–2.8 ka; Mitrovica *et al.* 2000). This difference is important, because whereas a single relaxation time is used to represent the whole Hudson Bay region in the formal Bayesian inversion leading to the VM2 radial viscosity model (of which VM5a is a 5-layer approximation) (Mitrovica & Peltier 1995; Peltier 1998c), the inversion performed by Mitrovica & Forte (2004) that leads to the FM family of viscosity profiles uses two different relaxation times for the area. Given that these regions are in such geographical proximity this would appear to be unphysical.

A further contribution to this debate was provided by Dyke & Peltier (2000), who revisited the exponential model RSL curve to qualitatively assess the impact of having various types of sea level indicators, in particular with respect to ^{14}C-dated mollusc shells whose habitat could extend (for many species) to a significant depth beneath mean sea level. However, the revised relaxation times produced by this analysis, which were around 2.5 ka, further exacerbated the misfit between the observed relaxation time and model predictions based upon the ICE-4G loading history coupled to the VM2 viscosity profile.

An important recent additional perspective is provided by the work of Pendea *et al.* (2010), who have published the first marine-to-freshwater transition shoreline displacement model for the James Bay area using accelerator mass spectrometry (AMS) dating of organic material in palaeo-tidal wetlands as emergence indicators. As pointed out by Pendea *et al.* (2010), the isolation basin methodology had been used in the past for individual lakes in the Hudson Bay region (Saulnier-Talbot & Pienitz 2001; Miousse *et al.* 2003), but not using a sequence of distinct basins, and never reaching as far south as James Bay. A similar methodology had previously been applied to great effect by Shennan *et al.* (1994) in constructing

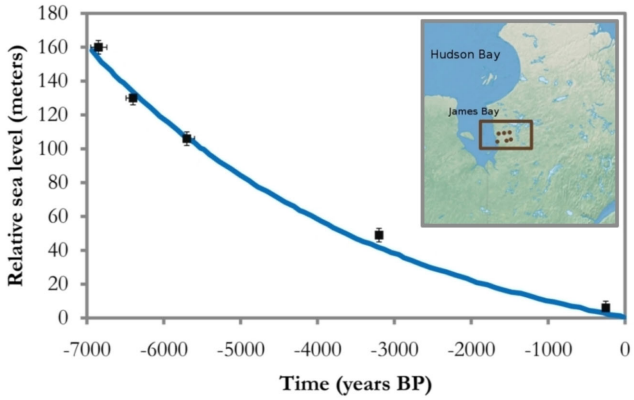

Figure 7. High quality sea level index points from the Pendea *et al.* (2010) analysis in the eastern part of James Bay, and the exponential decay fit that best represents the relaxation of the area after its deglaciation. The locations used in the Pendea *et al.* (2010) analysis are shown in the inset.

Table 1. Relaxation times determined in Eastern James Bay for various viscosity profiles coupled with the ICE-6G_C ice loading history.

Viscosity profile	Relaxation time (yr)	2σ uncertainty range (yr)	Reduced χ^2 of the fit
VM5a	4130	±50	0.9980
VM5b	3320	±70	0.9995
V1 (FM)	5700	±300	0.9988
V2 (FM)	6400	±400	0.9985
Pendea *et al.* (2010) data	3900	±800	0.91

the RSL history record for the Arisaig location and other sites in western Scotland. The data set of Pendea *et al.* (2010) provides an independent take on the debate concerning relaxation times in the James Bay area, and is significant since the methodology it employs is highly accurate. The location of the individual sites included in their analysis is shown in Fig. 7. Following Peltier (1998c), we have fit a simple exponential decay curve to the Pendea *et al.* (2010) data, while constraining it to zero modern-day change in relative sea level $S(t)$, following eq. (8):

$$S(t) = A[e^{t/\tau} - 1], \tag{8}$$

where τ is the inferred relaxation time and A is the amplitude characterizing the postglacial RSL history. This best fit, along with the Pendea *et al.* (2010) data, is presented in Fig. 7. A relaxation time of 3.9(±0.8) ka is obtained for this site. This result is noteworthy, as it calls into question the validity of the lower estimates for relaxation times for the area, such as the estimates of Dyke & Peltier (2000) as well as that of Mitrovica *et al.* (2000).

A comparison of the various *a posteriori* predictions of relaxation time for the various radial viscosity profiles under discussion in this analysis is presented in Table 1, and is very important given the new relaxation time inferred from the Pendea *et al.* (2010) record. First we note that the relaxation time for the Hudson Bay region predicted by VM5a is approximately 4.1 ka, which is the same as the prediction for VM2. This is expected since VM5a is a 5-layer approximation to the VM2 profile. Understandably, VM5b, which has an upper mantle half as viscous as VM5a, exhibits a much lower relaxation time than the other stiffer models. It is important to note that all of the previous Toronto models have relaxation times that are within the new observational inference obtained from the Pendea *et al.* (2010) data. On the other hand, the FM family of models exhibits relaxation times that are much higher than the other

models, with values of approximately 5.7 ka for V1 (FM) (a similar value to Mitrovica & Forte (2004)), and 6.4 ka for V2 (FM). These high values are due to the excessively high lower mantle viscosity that is delivered by the inversion procedure when a high relaxation time is assumed to govern the rebound process in the region near the centre of the Laurentide ice sheet. The FM family of models fails to predict relaxation times that fall within the error on the relaxation time estimated from the highly accurate isolation basin record of Pendea *et al.* (2010) as well as the previous estimates in Peltier (1998c).

Our initial observations strongly suggested that neither of the FM models (V1 and V2) are plausible insofar as understanding of the GIA process along the U.S. East coast is concerned when combined with the realistic ICE-6G_C loading history (especially along the southernmost portion of this coast). This view is now reinforced by the fact that these models also deliver excessively high relaxation times for the James Bay area. Although the claim was that the V1 and V2 models were constrained to fit both GIA and convection related constraints, it seems clear that they are not in fact able to explain GIA observables.

5.4 Case study I: Mantle viscosity variations in the upper mantle

Rather than further mining the existing literature for additional alternative models of mantle viscosity that might be employed to reconcile observations of relative sea level history with GIA model predictions along the U.S. East coast, we prefer to proceed by performing a systematic exploration of the sensitivity of model predictions to mantle viscosity variations at different depths. It is well-known that, for regions previously located beneath a former ice sheet and therefore undergoing uplift today, the sensitivity of the characteristic relaxation time for uplift of the crust depends strongly on the horizontal scale of the previously ice-covered region (e.g. Peltier 1998c), but the sensitivity to mantle viscosity variations is more complex for regions located in the surrounding glacial forebulge region, as the variation of viscosity with depth strongly impacts both the extent and amplitude of the forebulge itself (Tushingham & Peltier 1991).

The viscosity of the upper mantle and transition zone is known to have a profound impact on RSL predictions associated with ice sheets of moderate horizontal extent, such as the Fennoscandian ice sheet (Shennan *et al.* 2002). In the context of the larger Laurentide ice sheet, the impact is expected to be focused on the region in the ice sheet periphery. We have investigated a wide range of upper mantle and transition zone viscosity structures, and a representative subset of this family of models is presented here in Fig. 8, where upper mantle and transition zone viscosity values are varied from 0.25×10^{21} Pa s (the VM5b model of Engelhart *et al.* 2011) to 0.75×10^{21} Pa s, in a layer between the 660-km discontinuity and the base of the rheologically-stratified lithosphere (100 km depth), while the remainder of the radial viscosity structure is assumed to be identical to that of the VM5a profile. The RSL evolution predictions resulting from these models when combined to the ICE-6G_C loading history are presented in Fig. 8 for representative locations on the U.S. East coast (predictions for the full set of locations can be found in Fig. S2). A quantitative estimate of the error in the fit to the observational data is provided in Table S1.

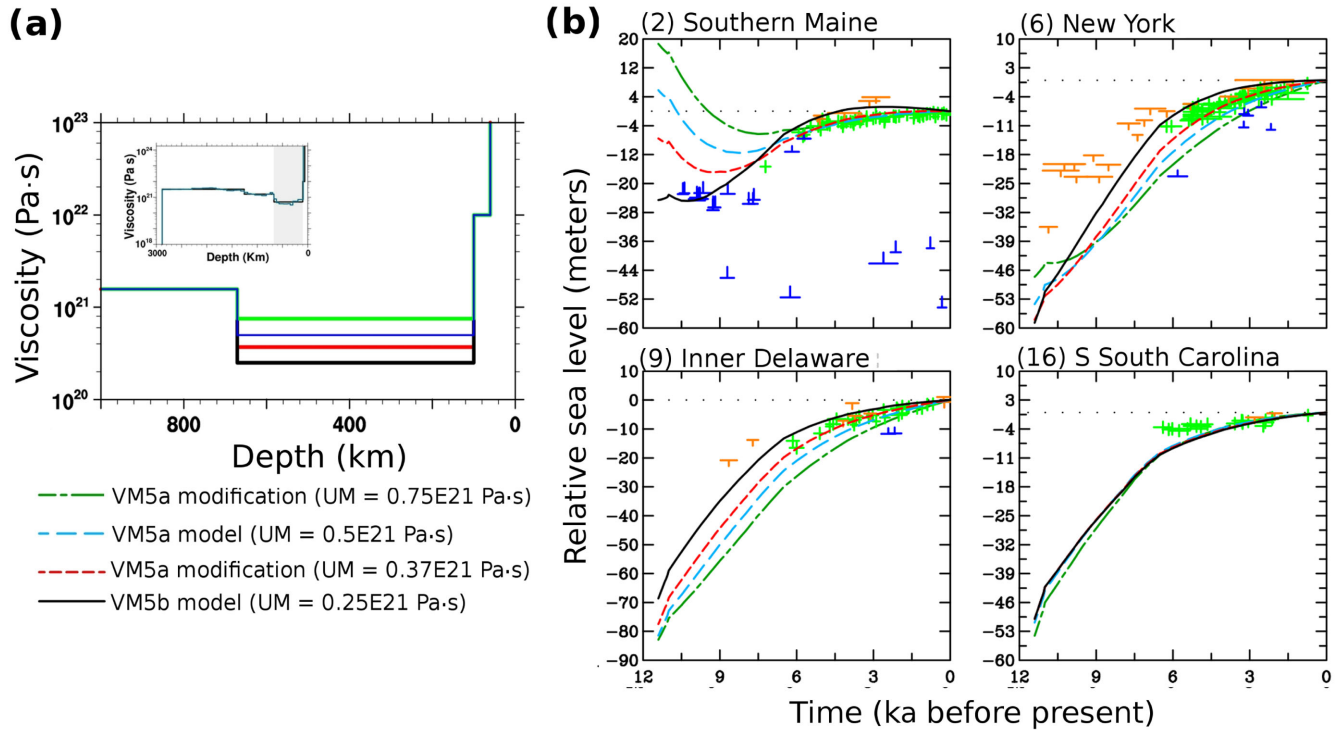

Figure 8. Comparison of a subset of regions of the Engelhart *et al.* (2011) data set of relative sea level histories along the U.S. Atlantic coast with the predicted relative sea level history at those locations for the ICE-6G_C model of ice-loading history combined to viscosity profiles where the viscosity of the upper mantle (UM) is allowed to vary (as discussed in the text). (a) Viscosity variations for the upper mantle (values are shown in the legend). The region of the mantle in which the variations occur is highlighted in the inset. (b) For the models shown in (a), comparison of RSL history predictions with observational data at four locations of the Engelhart *et al.* (2011) data set, namely Southern Maine (2), New York (6), Inner Delaware (9) and Southern South Carolina (16). Green data points represent sea level index points, whereas blue crosses represent marine-limiting data and orange crosses represent terrestrial-limiting data.

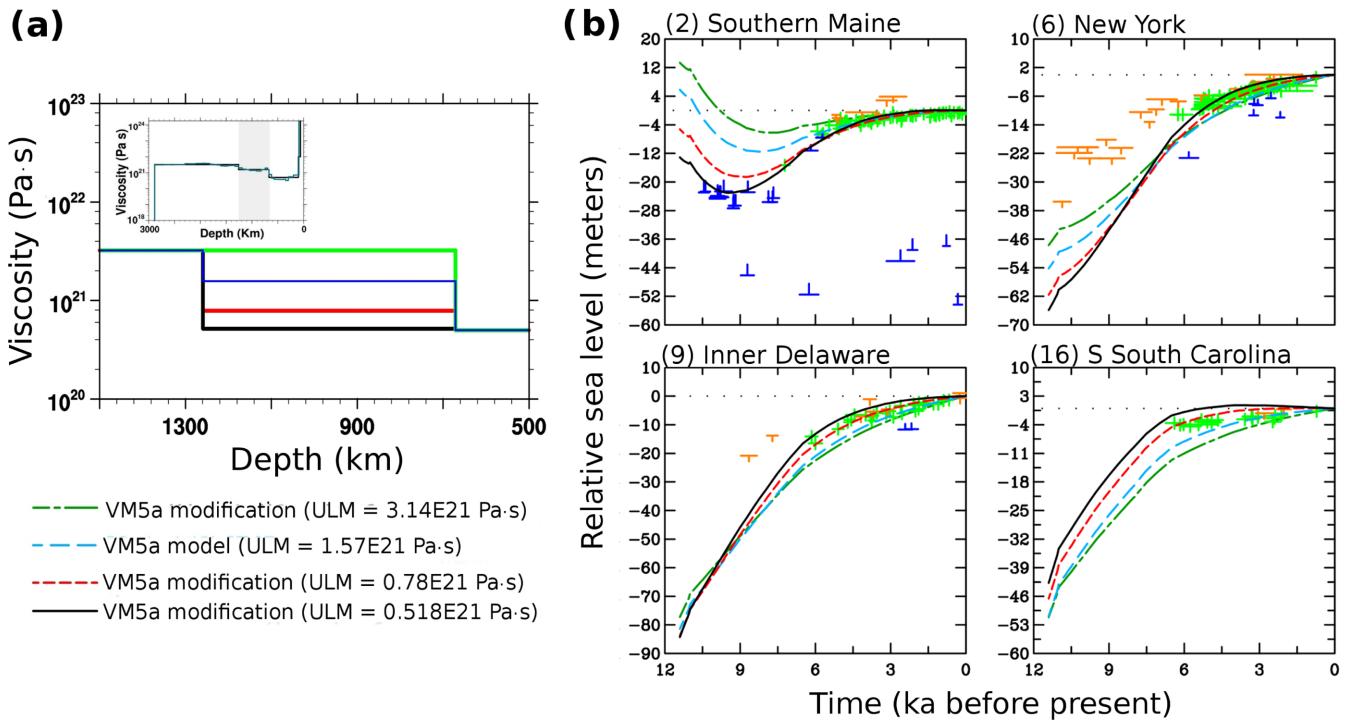

Figure 9. Comparison of a subset of regions of the Engelhart *et al.* (2011) data set of relative sea level histories along the U.S. Atlantic coast with the predicted relative sea level history at those locations for the ICE-6G_C model of ice-loading history combined to viscosity profiles where the viscosity of the upper part of the lower mantle (ULM) is allowed to vary (as discussed in the text). (a) Viscosity variations for the upper part of the lower mantle (values are shown in the legend). The region of the mantle in which the variations occur is highlighted in the inset. (b) For the models shown in (a), comparison of RSL history predictions with observational data at four locations of the Engelhart *et al.* (2011) data set, namely Southern Maine (2), New York (6), Inner Delaware (9) and Southern South Carolina (16). Green data points represent sea level index points, whereas blue crosses represent marine-limiting data and orange crosses represent terrestrial-limiting data.

Varying progressively the value of the viscosity in the upper mantle and transition zone from 0.25×10^{21} to 0.75×10^{21} Pa s results in a broad but consistent range of predictions. Focusing first on the northernmost locations, the viscosity of the target region strongly impacts the predictions of RSL evolution. Models characterized by a more viscous upper mantle have reduced forebulge amplitudes which develop later in time, while models with less viscous upper mantles recover significantly more quickly towards equilibrium. Progressing further south into the forebulge, softer models such as VM5b perform better at reconciling GIA predictions and observations, especially for the most recent 4 ka. However, beginning in North Carolina, such variations in mantle viscosity fail to explain the older data, and by South Carolina, relative sea level history predictions become insensitive to variations of viscosity in the target region. However, it should be noted that the spectrum of Fennoscandian relaxation times is highly sensitive to the viscosity in the region above the 660 km seismic discontinuity (Peltier 1998c), so much so that the fit to this spectrum constitutes a crucial test of any spherically symmetric viscosity model.

5.5 Case study II: Viscosity variations in the upper part of the lower mantle

Given the large horizontal scale of the Laurentide Ice sheet, it is known that the site-specific Fréchet derivatives associated with the surface relaxation beneath the former ice sheet are highly sensitive to mantle viscosity variations in the upper part of the lower mantle (e.g. Peltier & Andrews 1976; Peltier & Jiang 1996; Peltier 1998c; Wu *et al.* 2010). This sensitivity can be expected to extend into the peripheral bulge region associated with the former Laurentide ice sheet, and to impact not only the geographical extent of the forebulge, but also its temporal evolution. We have investigated the sensitivity of RSL predictions along the U.S. East coast to a wide range of variations in the viscosity of the upper part of the lower mantle, and in a representative subset of those models, the viscosity of the upper part of the lower mantle has been taken to vary over the range from 0.518×10^{21} Pa s (one third of the value of the viscosity of the VM5a model in this region), through the sequence 0.78×10^{21} Pa s, 1.57×10^{21} Pa s (the VM5a profile) and 3.14×10^{21} Pa s, while the viscosity structure of the rest of the mantle is kept fixed to that of the VM5a profile. Fig. 9 compares the RSL predictions resulting from these variations of the VM5a structure when combined to the ICE-6G_C ice loading history for the same subset of locations from Engelhart *et al.* (2011) as employed previously. Comparisons to the complete data set are found in the Supplementary material section (Fig. S3). Based on these results, it follows that in the northernmost regions of the coast, the softer models produce a peripheral bulge of larger amplitude that reaches its maximum earlier following initiation of the deglaciation process. Moving further south along the coast reveals that this difference increases in magnitude, and leads to the presence of a mid-Holocene high stand south of Virginia for the softest of the models analysed, a feature that is incompatible with the RSL data from the region. From these observations, when compared to the predictions for the VM5a viscosity structure, a lower viscosity in the upper part of the lower mantle would be expected to partly eliminate the misfits observed along the southern part of the U.S. East Coast, although the optimal viscosity must be high enough to

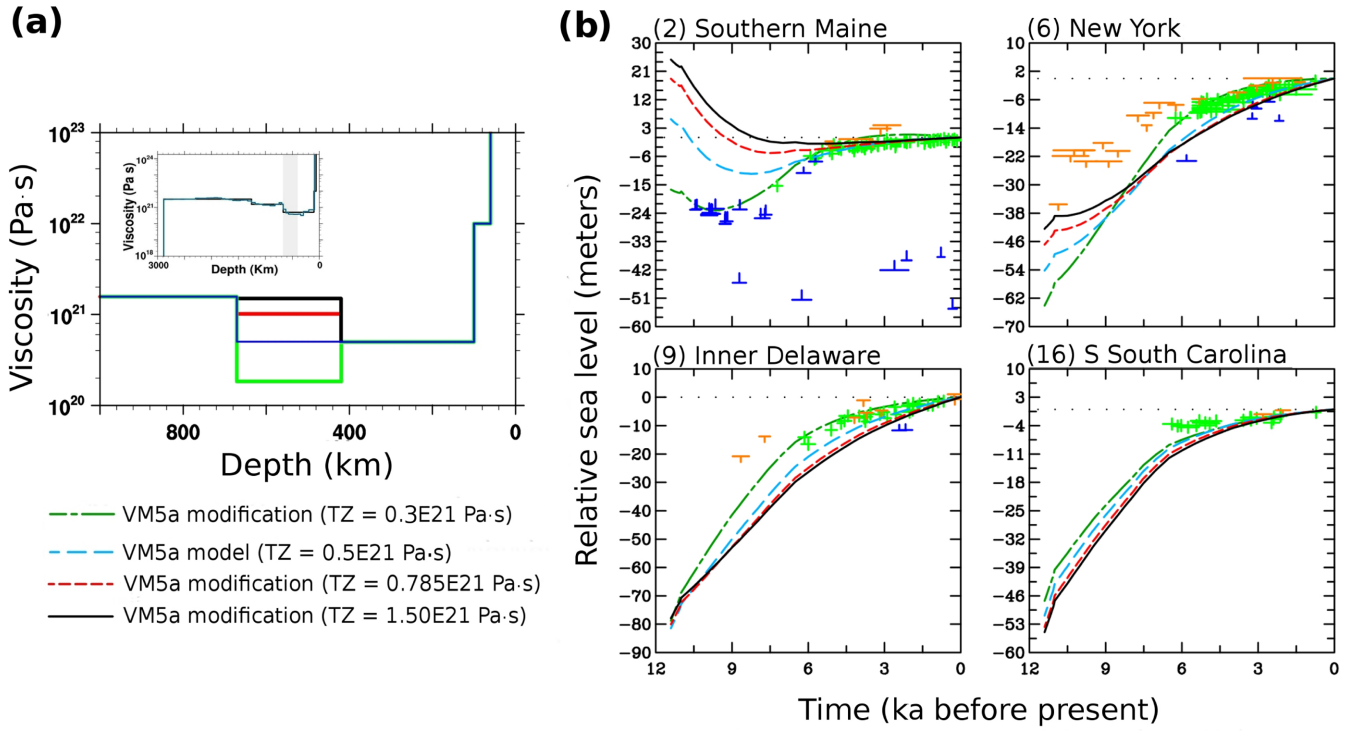

Figure 10. Comparison of a subset of regions of the Engelhart *et al.* (2011) data set of relative sea level histories along the U.S. Atlantic coast with the predicted relative sea level history at those locations for the ICE-6G_C model of ice-loading history combined to viscosity profiles where the viscosity of the transition zone (TZ) is allowed to vary (as discussed in the text). (a) Viscosity variations for the transition zone (values are shown in the legend). The region of the mantle in which the variations occur is highlighted in the inset. (b) For the models shown in (a), comparison of RSL history predictions with observational data at four locations of the Engelhart *et al.* (2011) data set, namely Southern Maine (2), New York (6), Inner Delaware (9) and Southern South Carolina (16). Green data points represent sea level index points, whereas blue crosses represent marine-limiting data and orange crosses represent terrestrial-limiting data.

prevent the formation of high stands in the regions south of Virginia and at Barbados.

5.6 Case study III: Viscosity variations in the transition zone

When characterizing the sensitivity of RSL history predictions to mantle viscosity, a further avenue that warrants explicit study concerns the possibility of the existence of a harder transition zone between depths of 410 and 660 km, as has been previously shown to trade off perfectly with a softening of viscosity in the vicinity of the deeper endothermic phase transition itself (e.g. Peltier 1998c). Because the mineral assemblage present in the transition zone is especially rich in garnet, there are *a priori* reasons to believe that a feature of this kind in the depth dependence of mantle viscosity could exist. However, the recent discovery of ringwoodite, a high-pressure polymorph of olivine thought to originate in the transition zone, imbedded in a diamond from a Brazilian diamond pipe (Pearson *et al.* 2014) suggests that viscosity of the transition zone might instead be lower than the viscosity of the upper mantle, since ringwoodite is a hydrous phase and the observation might be interpreted to suggest that the transition zone is rich in water. In the context of the GIA response to the melting of the Laurentide ice sheet over the East coast of North America, modifying the viscosity structure in this region alone and not in the upper mantle could result in a change in the characteristics of the forebulge, while also modifying somewhat the ability of the model to fit the Fennoscandian relaxation spectrum.

To investigate the impact of viscosity variations in the transition zone on sea level dynamics in the glacial forebulge region, we have once again looked at a sequence of modifications of the VM5a profile. These new models are identical to the VM5a profile, except in the channel between the base of the transition zone at 660 km depth and the top of the transition zone at 410 km depth, a region in which the effective viscosity is varied from 0.30×10^{21} to 1.50×10^{21} Pa s. The impact of these variations on RSL predictions for the subset of locations along the U.S. East coast is shown in Fig. 10 (with the full set of comparisons found in the Supplementary Material section, in Fig. S4). In the northern and central regions of the coast, increasing the viscosity in the channel between the depths of 410 and 660 km creates a less pronounced forebulge that achieves its maximum displacement at a later time. In these regions, a softer transition zone seems to be favoured when comparing to sea level index point data, although stiffer models enable a slightly better fit to the marine-limiting observational data at some locations (e.g. Massachusetts). The difference between the predictions resulting from the stiffer viscosity profiles is quite limited for sites in the mid-Atlantic regions (such as Connecticut and New York), but the soft transition zone models perform notably better in those regions. Indeed, for New Jersey, Delaware, Virginia and the index points of the Chesapeake Bay record, the softer transition zone models provide a better fit to the observational data provided in the Engelhart *et al.* (2011) database. For regions further south, the inter-model comparison differences become less important. One explanation for this behaviour could be that, as the viscosity under the lithosphere is decreased, the geographical extent of the forebulge decreases, a feature that is accompanied by a larger amplitude of response at locations closer to the former Laurentide ice sheet.

Correspondingly, for models with a stiffer transition zone, the impact of the forebulge is felt further south along the eastern U.S. seaboard, and the predicted RSL curves for those models are shifted to shallower depth compared to the original VM5a model and with less curvature in the recovery phase. Hence, increasing the viscosity in the transition zone provides a poorer fit to the RSL observations for most locations along the U.S. East coast. Thus, large changes in mantle viscosity in the transition zone would have to be incorporated simultaneously with large viscosity changes in either the upper mantle or the upper part of the lower mantle to account for the RSL evolution misfits introduced in the northernmost and southernmost parts of the U.S. East coast.

5.7 Case study IV: Viscosity contrast variations between the upper mantle and lower mantle

Most simple models of mantle viscosity include a discontinuity in mantle viscosity associated with the presence of the 660-km seismic discontinuity (e.g. Peltier 1989), and the issue of determining an appropriate contrast between the upper and lower mantle is explored here in the context of relative sea level evolution predictions for the Eastern seaboard of the United States. Results for a representative subset of viscosity structures are shown here, where two different viscosity values are explored for both the upper part of the lower mantle (1.57×10^{21} and 0.785×10^{21} Pa s) and for the upper mantle and transition zone (0.75×10^{21} and 0.37×10^{21} Pa s), which results in four different viscosity structure combinations.

Fig. 11 presents the relative sea level history predictions resulting from these structures for the subset of representative locations on the U.S. East coast (a full complement of comparisons for all sites can be found in the Supplementary material section, in Fig. S5). Beginning with the northernmost locations, it is noticeable that for the lowest upper mantle and transition zone viscosity (0.37×10^{21} Pa s), increasing the contrast between the upper and lower mantle (by increasing the value of the lower mantle viscosity) leads to a less prominent forebulge that reaches its maximum amplitude at a slightly later time, a direct consequence of the slower mantle material flow caused by its higher overall viscosity. In terms of relative sea level evolution at the locations of interest on the U.S. East coast, this increase of the lower mantle viscosity results in flatter sea level curves and slower recovery to today's observed sea level. Repeating the analysis for a higher upper mantle viscosity (0.75×10^{21} Pa s), a similar behaviour is observed for the northernmost sites. However, for mid-Atlantic sites (Massachusetts to Maryland), the higher upper mantle viscosity masks any impact arising from a higher lower mantle viscosity. In Virginia and the Carolinas, as was the case for the models with the lower upper mantle and transition zone viscosity, relative sea level history predictions are highly dependent on the value of lower mantle viscosity employed. Models with softer lower mantles tend to reproduce the observational data of Engelhart *et al.* (2011) more accurately, although in the two sets of experiments shown here, the overall sea level evolution curvature is not captured accurately.

5.8 Case study V: Lithosphere thickness variations

Another important sensitivity analysis concerns the thickness of the elastic lithosphere. Here, lithospheric thickness is varied from 60 to

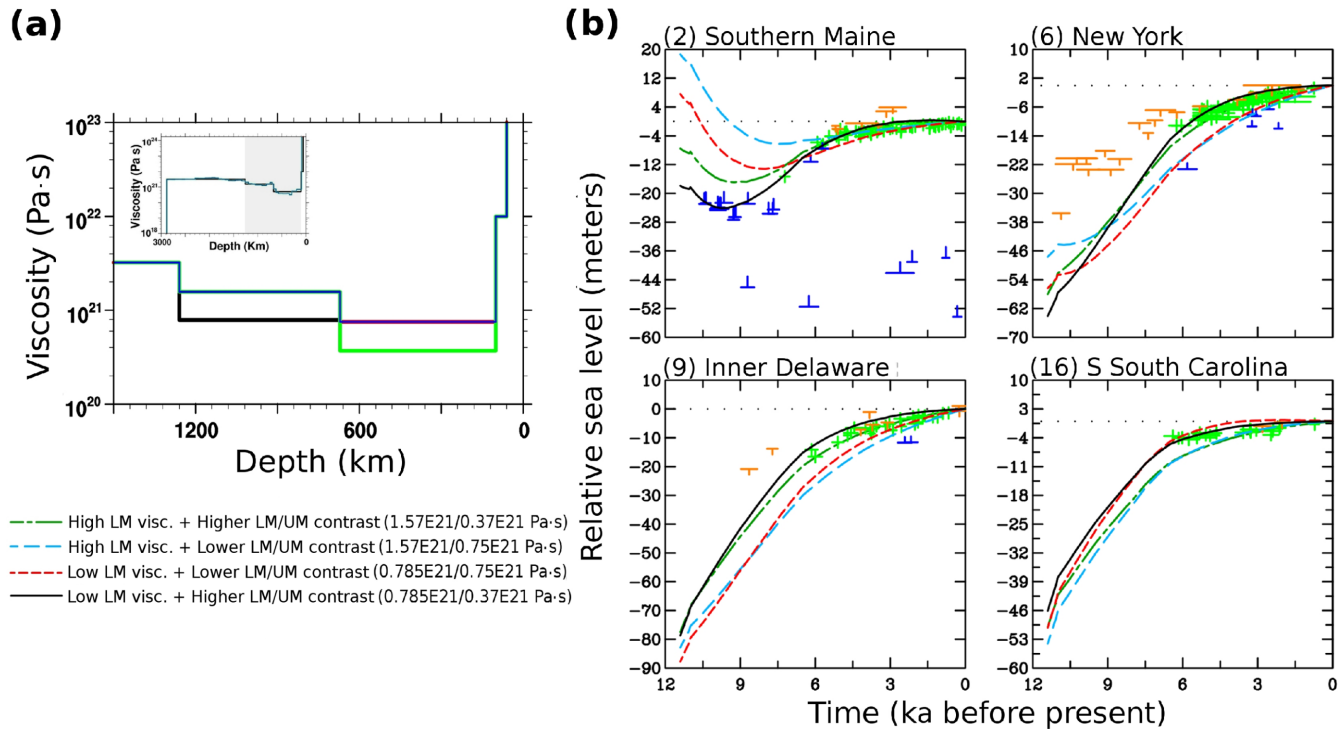

Figure 11. Comparison of a subset of regions of the Engelhart *et al.* (2011) data set of relative sea level histories along the U.S. Atlantic coast with the predicted relative sea level history at those locations for the ICE-6G_C model of ice-loading history combined to viscosity profiles where the viscosity contrast between the upper and lower mantles is allowed to vary (as discussed in the text). (a) Upper/lower mantle viscosity contrast variations (values are shown in the legend). The region of the mantle in which the variations occur is highlighted in the inset. (b) For the models shown in (a), comparison of RSL history predictions with observational data at four locations of the Engelhart *et al.* (2011) data set, namely Southern Maine (2), New York (6), Inner Delaware (9) and Southern South Carolina (16). Green data points represent sea level index points, whereas blue crosses represent marine-limiting data and orange crosses represent terrestrial-limiting data.

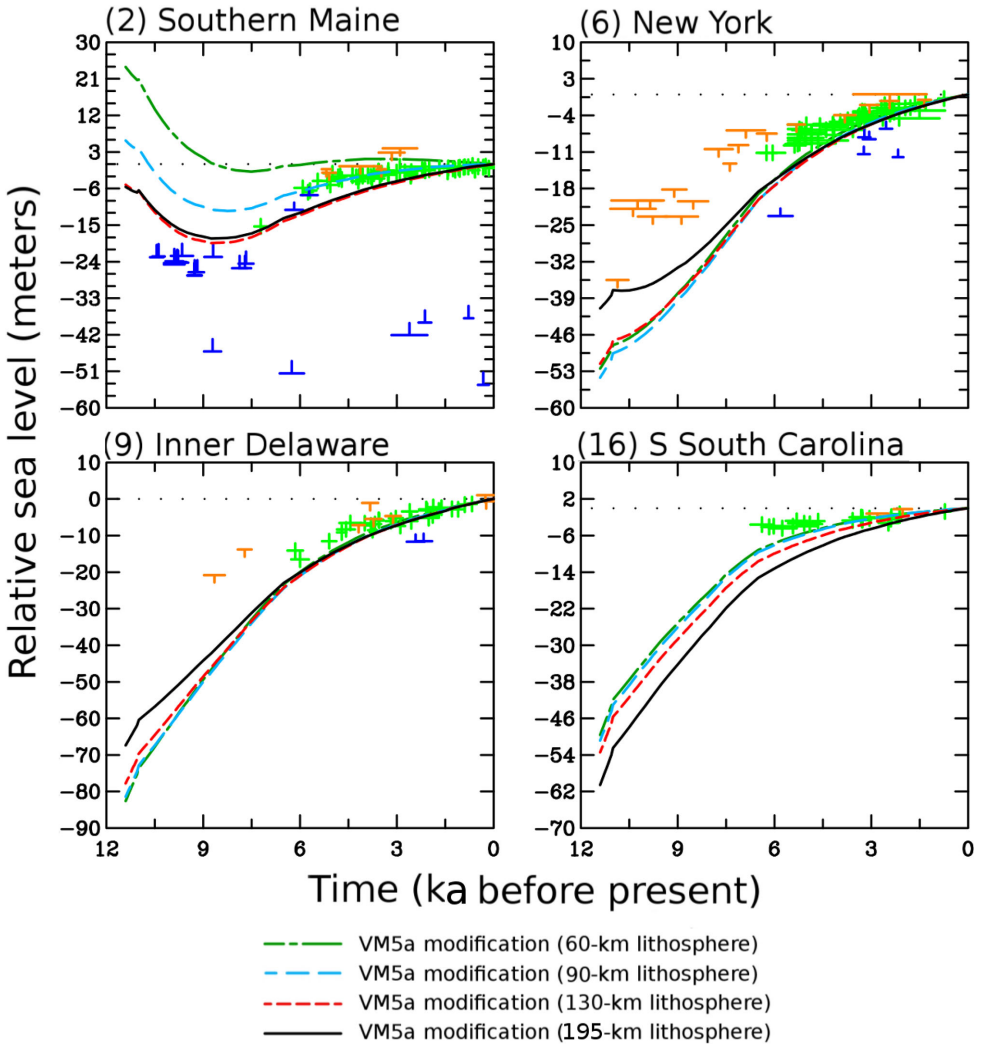

Figure 12. Comparison of a subset of regions of the Engelhart *et al.* (2011) data set of relative sea level histories along the U.S. Atlantic coast [Southern Maine (2), New York (6), Inner Delaware (9) and Southern South Carolina (16)] with the predicted relative sea level history at those locations for the ICE-6G_C model of ice-loading history combined to viscosity profiles where the thickness of the elastic lithosphere is allowed to vary (as discussed in the text). Green data points represent sea level index points, whereas blue crosses represent marine-limiting data and orange crosses represent terrestrial-limiting data.

195 km (through the sequence of 60, 90, 130 and 195 km), while the rest of the mantle viscosity structure is fixed to the VM5a profile. The rheological stratification of the lithosphere present in the VM5a and VM5b viscosity profiles is ignored in this test. Relative sea level evolution predictions for the U.S. East coast are compared to the sea level indicators of Engelhart *et al.* (2011), and are shown for the 16 regions of the data set in the Supplementary Material section (Fig. S6), while results for a subset of four regions are shown in Fig. 12.

The model predictions for the northernmost sites (in particular Eastern and Southern Maine) are particularly interesting. While the forebulge is almost absent when using models with a very thin lithosphere, as lithospheric thickness is increased from 60 to 130 km, the forebulge gains in maximal amplitude and reaches it at earlier times. However, the behaviour becomes less marked for a thicker lithosphere (or even slightly reverses for the thickest lithospheres considered), which implies that there might be a lithospheric thickness value that maximizes the amplitude of the local forebulge for the northernmost sites. Similarly, progressing further south along the coast, models with a thinner lithosphere are characterized by a wide range of predictions, but models with very thick elastic lithospheres (130 km and above) display a similar RSL evolution. In the mid-Atlantic region (e.g. New York and Inner Delaware), this situation manifests itself in the form of a forebulge of lower amplitude for the thickest lithosphere under consideration. Conversely, in the southernmost regions, models with a thin lithosphere exhibit a similar behaviour, while the viscosity structures with a thicker lithosphere display a broader range of predictions with a more prominent forebulge, a feature which is not desirable given the small change in RSL history over the past 6 ka captured by the sea level indicators in the region.

This series of features can be explained in terms of the physical nature of the movement of mass in the mantle associated with the former Laurentide ice sheet and the corresponding flexure of the lithosphere it induces. For a thicker lithosphere, the greater stiffness of the Earth's solid surface tends to spread the forebulge over a larger geographical area, while diminishing its maximal amplitude. Viscosity models with thinner lithospheres result in more pronounced, but more localized, glacial forebulges. In this context, as different lithospheric thicknesses have competing effects for various regions along the U.S. East coast, a simple variation of this parameter does not provide a satisfactory improvement in the

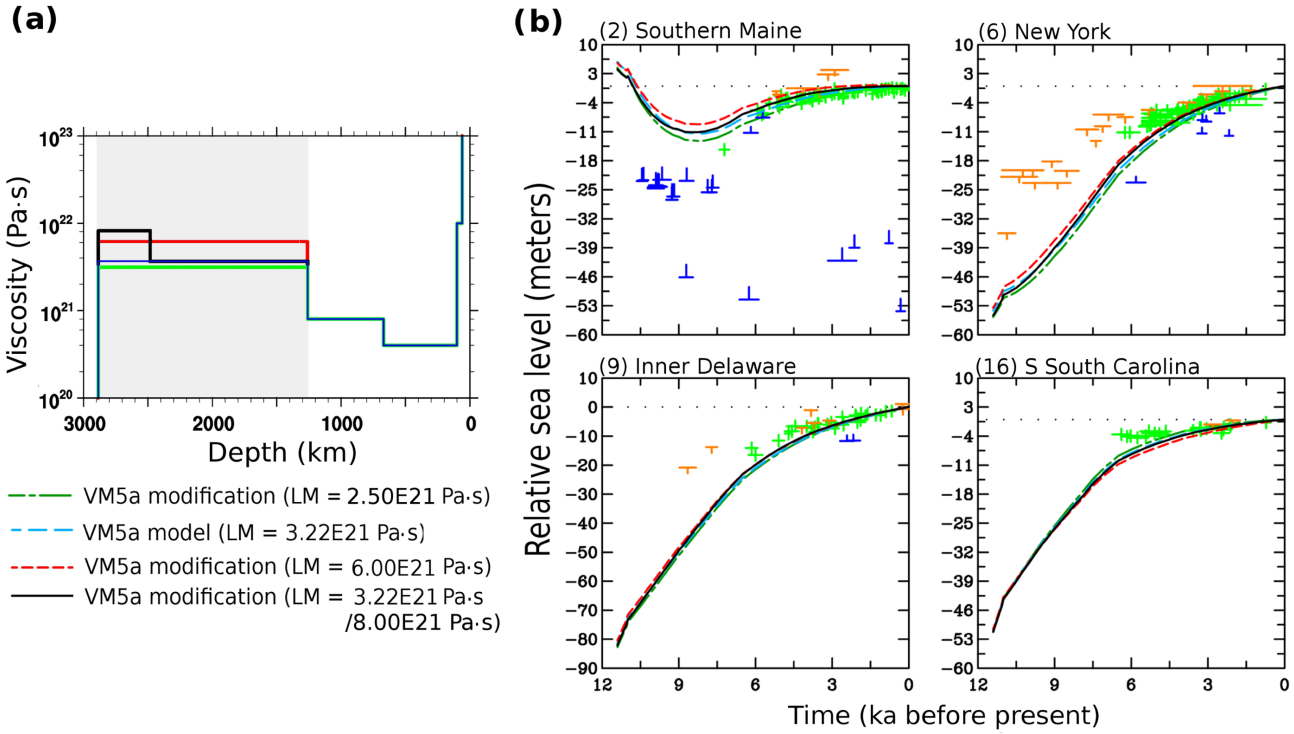

Figure 13. Comparison of a subset of regions of the Engelhart *et al.* (2011) data set of relative sea level histories along the U.S. Atlantic coast with the predicted relative sea level history at those locations for the ICE-6G_C model of ice-loading history combined to viscosity profiles where the viscosity of the lower part of the lower mantle is allowed to vary (as discussed in the text). (a) Viscosity variations in the lower part of the lower mantle (values are shown in the legend). (b) For the models shown in (a), comparison of RSL history predictions with observational data at four locations of the Engelhart *et al.* (2011) data set, namely Southern Maine (2), New York (6), Inner Delaware (9) and Southern South Carolina (16). Green data points represent sea level index points, whereas blue crosses represent marine-limiting data and orange crosses represent terrestrial-limiting data.

ability of the VM5a viscosity profile to explain the RSL observational data over all regions along the coast.

5.9 Case study VI: Lower mantle viscosity variations and the Earth's rotational state

It has been long established that the Earth's rotational state continues to be influenced by the isostatic adjustment of the planet resulting from the deglaciation process that followed LGM (e.g. Peltier 1982; Wu & Peltier 1984; Peltier 1996a), in particular concerning the two main rotational anomalies observed today: the non-tidal acceleration of the rate of planetary rotation and the secular drift of the pole of rotation with respect to the surface of the planet (true polar wander). Modern observations of these anomalies are numerous: in fact, changes in the non-tidal acceleration of the planetary rotation rate can be observed in the change of oblateness of figure of the planet from careful measurements of the evolution of satellite orbital parameters (e.g. Yoder *et al.* 1983; Cheng & Tapley 2004; Roy & Peltier 2011; Cheng *et al.* 2013) or in historical records of the timing of lunar and solar eclipses (Stephenson & Morrison 1995). Changes in the secular drift of the pole can be observed from space-geodetic techniques, such as very long baseline interferometry (VLBI), global positioning system (GPS) measurements, and lunar and satellite laser ranging (SLR; e.g. Gross & Vondrák 1999; Roy & Peltier 2011; Ratcliff & Gross 2013).

The ability of a GIA model to reproduce historical values of these rotational anomalies is an important test of its validity. In particular, predictions of these GIA-induced anomalies are mostly sensitive to the viscosity of the lowermost mantle (e.g. Peltier 1982; Wu & Peltier 1984). More importantly, predictions of RSL evolution following the deglaciation were found to be sensitive to the viscosity of the upper part of the lower mantle but only weakly sensitive, if at all, to changes in the viscosity of the deepest portion of the lower mantle (Peltier 1998c). In this context, to explain the rotational anomalies observed today, it might be necessary to adjust the value of the viscosity in the lower part of the lower mantle, given the implications of the previously discussed sensitivity analyses that a reduction of mantle viscosity in the upper part of the lower mantle appears to be required to improve the quality of GIA predicted RSL histories along the southern part of the U.S. East coast. It is therefore important to investigate the impact of such viscosity changes in the deepest mantle on RSL predictions, if any, as these modifications might be required to maintain the quality of fit to Earth rotation constraints when an appropriately softened shallower structure is introduced. In Fig. 13, predictions of RSL evolution for four key sites along the U.S. East coast are presented when the viscosity of the lowermost lower mantle is allowed to vary uniformly between three different values illustrated in panel (a) (the comparison to the observational data in all 16 sites is shown in Fig. S7). We also investigate the impact of constraining a potential viscosity increase to the lowermost section of the lower mantle. The panels shown in Fig. 13(b) demonstrate the minimal impact induced on RSL evolution predictions by slight changes in lower mantle viscosity, with the only notable difference seen at the very edge of the former Laurentide ice sheet in Maine. Furthermore, by concentrating the increase in lower mantle viscosity to the very deepest part of the mantle and keeping the rest of the viscosity structure fixed to VM5a, it should be noted that the RSL predictions are identical to the ones made using the VM5a structure.

5.10 Other considerations and a summary of the insights gained through the sensitivity analyses

Synthesizing the results of these calculations, it appears that for the ICE-6G_C ice loading model several possible combinations could lead to a good fit to RSL observations in the northernmost locations along the U.S. East coast. Indeed, for these regions, the thickness of the elastic lithosphere and the viscosity of the upper mantle and transition zone have an important influence on the RSL predictions, while the viscosity of the upper part of the lower mantle has a significant impact on the shape of the forebulge and its decay. However, the RSL data from the southern part of the U.S. East coast is only better represented with a viscosity in the upper part of the lower mantle that is slightly lower than that characteristic of the VM2 and VM5a profiles, which reduces the ambiguity as to which of the possible combinations one should first apply to better fit the data from the northernmost points along the coast. For instance, an increase in lithospheric thickness decreases the quality of the fit in the southernmost locations while a reduction of its thickness does not reconcile RSL observations with the model predictions, which restricts the range of possibilities in the quest for an improved model that will enable us to fit the majority of the observational data. The case of the transition zone is particularly interesting. As discussed previously, changes in the viscosity of the transition zone have some impact on RSL predictions at northern locations along the U.S. East coast, and a softer transition zone fits the mid-Atlantic data points better. However, another key impact of transition zone viscosity (and in the upper part of the mantle in general) relates to the ability of the viscosity model to fit the Fennoscandian spectrum of spherical harmonic degree-dependent relaxation times. As the viscosity of the upper part of the lower mantle must be decreased to fit the observational data from the southernmost locations along the U.S. East coast, viscosity changes in the transition zone might be necessary to maintain an adequate fit to the Fennoscandian spectrum if the viscosity decrease in the upper mantle proves to be too large. However, the introduction of a harder transition zone would not be preferred, as it would affect the quality of the fit to the geologically derived RSL data in the same locations that we are attempting to fit more accurately. Nonetheless, it is clear that the viscosity in the transition zone can be used as a fine-tuning parameter in balancing the quality of the fit to the Fennoscandian spectrum and to the geologically derived RSL data from the southernmost locations of the Engelhart *et al.* (2011) data set.

6 A PREFERRED VISCOSITY STRUCTURE: THE VM6 PROFILE

Combining the previous analyses, and using the most recent ICE-6G_C globally consistent ice loading history (Argus *et al.* 2014; Peltier *et al.* 2015), a new radially symmetric viscosity profile for the Earth's mantle that addresses the shortcomings of the VM5a and VM5b profiles is presented here. This new viscosity structure, which is referred to as VM6, is illustrated in Fig. 14(a) and its properties are listed in Table 2. It contains a rheological stratification of the lithosphere similar to the one introduced with the VM5a profile, but with a slightly thicker elastic lithosphere (90-km elastic lithosphere superimposed upon a 30-km-thick layer with higher than upper mantle viscosity, introduced to reconcile GIA model predictions of present-day horizontal motion of the solid Earth surface with space-geodetic observations (Peltier & Drummond 2008)). In the VM6 profile, the viscosity of the upper part of the mantle, located between the base of the lithosphere and the base of the transition zone at 660 km depth (0.45×10^{21} Pa s), lies between the viscosity of VM5a and VM5b. No additional structure in the transition zone (between the 420-km and 660-km seismic discontinuities) was found to be necessary to reproduce RSL histories based upon the observed sea level indicators in the Engelhart *et al.* (2011) data set, since the viscosity at this depth is also constrained by the need to maintain an adequate fit to the Fennoscandian spectrum. Instead, to maintain the fit to this set of observables, it was preferable to reduce the viscosity in the upper part of the lower mantle, where it is set to 0.9×10^{21} Pa s, or about half the viscosity characteristic of the VM5a structure in this region. The lower part of the lower mantle requires a slight decrease in viscosity, but prefers the addition of an extra layer of very high viscosity above the core–mantle boundary to maintain a good fit to the constraints provided by rotational observables. These modifications, suggested by the extensive search of parameter space we have performed, do enable the revised model to address decisively the shortcomings of the VM5a viscosity profile. The slightly softer upper mantle (including the transition zone) enables a better reconstruction of relative sea level histories in the mid-Atlantic sites of the Engelhart *et al.* (2011) data set of relative sea level indicators from the U.S. East coast. In particular, a decrease of the viscosity in the upper part of the lower mantle addresses the issue of the misfits identified between the observational data in the Carolinas and the model predictions for the VM5a and VM5b viscosity profiles identified by the same authors.

The fit to the Fennoscandian spectrum provided by the VM6 profile is shown in Fig. 14(b). The relaxation times inferred for the largest deformation scales are somewhat lower than for the VM5a profile (also shown), largely owing to the slight decrease in effective viscosity across much of the upper mantle (including the slight reduction in the transition zone) and the upper part of the lower mantle. However, they remain comfortably within the 2σ uncertainty range of the Fennoscandian spectrum suggested by the formal analysis of Wieczerkowski *et al.* (1999). While a higher viscosity in the transition zone would enable the inferred Fennoscandian relaxation times to remain within a 1σ uncertainty range for these longest horizontal scales, doing so would decrease the quality of the fit to RSL observations for a substantial number of sites along the U.S. East coast, most notably in the mid-Atlantic region. A slight reduction in mantle viscosity in the transition zone from the VM5a model, similar to the change applied to the rest of the upper mantle, was found to fit the observational data at these sites optimally. For higher spherical harmonic degrees (e.g. smaller deformation scales), the relaxation times for VM6 lie well within the 1σ uncertainty range. Thus, the VM6 viscosity profile increases not only the quality of the model fit to the northern and mid-Atlantic sites of the Engelhart *et al.* (2011) U.S. East coast relative sea level data set, but also eliminates almost completely the important misfits found by Engelhart *et al.* (2011) for the earlier part of the data records at the southern locations, while also fitting the strong constraint imposed upon the assumed spherically symmetric viscosity structure by the Fennoscandian relaxation spectrum.

6.1 The predictions for the U.S. East coast for ICE-6G_C (VM6)

Comparisons between the complete Engelhart *et al.* (2011) data set of relative sea level indicators and the ICE-6G_C (VM6) predictions of RSL history are shown in Fig. 15, while a summary of the changes in reduced χ^2 performance introduced by the new model when compared to the fit provided by the ICE-6G_C (VM5a) model

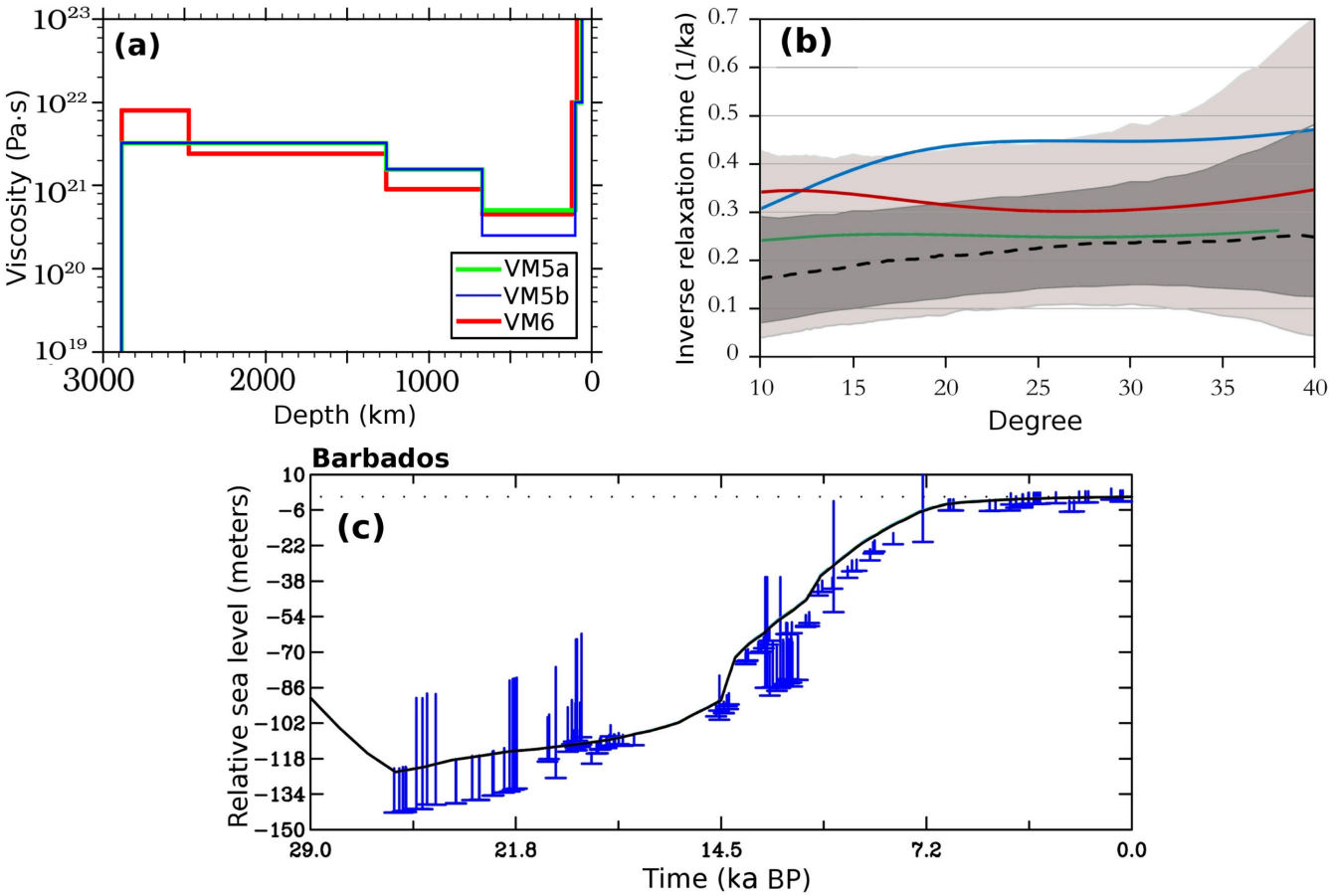

Figure 14. (a) Comparison of the radial variations of the viscosity in depth for the new VM6 viscosity profile (red) with the VM5a (green) and VM5b (blue) profiles. (b) Inverse relaxation time as a function of spherical harmonic degree obtained from observations of the glacial isostatic adjustment of Fennoscandia, with the relaxation spectrum (black) and corresponding 1σ uncertainties (solid grey lines) calculated by Wieczerkowski *et al.* (1999) (the grey dashed line uses a subset of the available strandline data). The predicted spectra for the new VM6 viscosity structure is shown in red, while the predictions for the VM5a (green) and VM5b (light blue) models are superimposed. (c) Fit of the ICE-6G_C model predictions to the Barbados record of coral-based sea level indicators when combined to the VM6 viscosity structure.

Table 2. Radial viscosity structure of the VM6 viscosity profile down to the core–mantle boundary.

Depth range (km)	Viscosity ($\times 10^{21}$ Pa s)
0–90	Elastic
90–120	10
120–420	0.45
420–670	0.45
670–1260	0.9
1260–2400	2.4
2400–2885.5	8

is shown in Table 3. For indicative purposes, the performance of the VM5b viscosity model is also included in Table 3 in italics. However, as demonstrated earlier, it should be noted that VM5b is not a favoured spherically symmetric model of mantle viscosity, as it is unable to explain other geophysical observables (such as the Fennoscandian spectrum of relaxation times), while VM6 can do so. For the northernmost sections of the U.S. East coast, VM6 provides a marginally improved fit to the observations over that of the VM5a profile only for the latest 4 ka of the observational record, while the earlier record is not well explained by VM6 (or VM5b), explaining the large decrease in performance seen in Table 3 for these northernmost locations. This behaviour is not unexpected, given the sensitivity of the RSL predictions in this region to the deglaciation history and the viscosity of the upper mantle. Since the region was co-located with the margin of the Laurentide ice sheet during the initial phases of the last deglaciation and is relatively close to a region of complex margin evolution (e.g. Borns *et al.* 2004), slight modifications to the ice loading history would be able to resolve this localized misfit. It should be noted, however, that VM6 provides an improved fit compared to VM5a for most of the sea level index points south of Connecticut. In particular, in New York (site 6), VM6 provides a fit to the observational data much superior to both VM5a and VM5b, especially for the more recent sea level index points. For Long Island and New Jersey (sites 7 and 8), the change in viscosity structure from VM5a to VM6 improves the fit to the more recent index points, but does not provide a substantial improvement for indicators older than 4 ka. The performance difference observed between VM5a and VM6 (or between VM5b and VM6) in Long Island (site 7) is strongly affected by a few outlying data points (mostly marine-limiting) that none of the models can explain, and which dominate the percentage change shown in Table 3 for these locations. Progressing further south, the VM6 model is found to be much superior to VM5a, increasing substantially the quality of the fit of the GIA model to the Engelhart *et al.* (2011) data set in Maryland, Virginia and Delaware

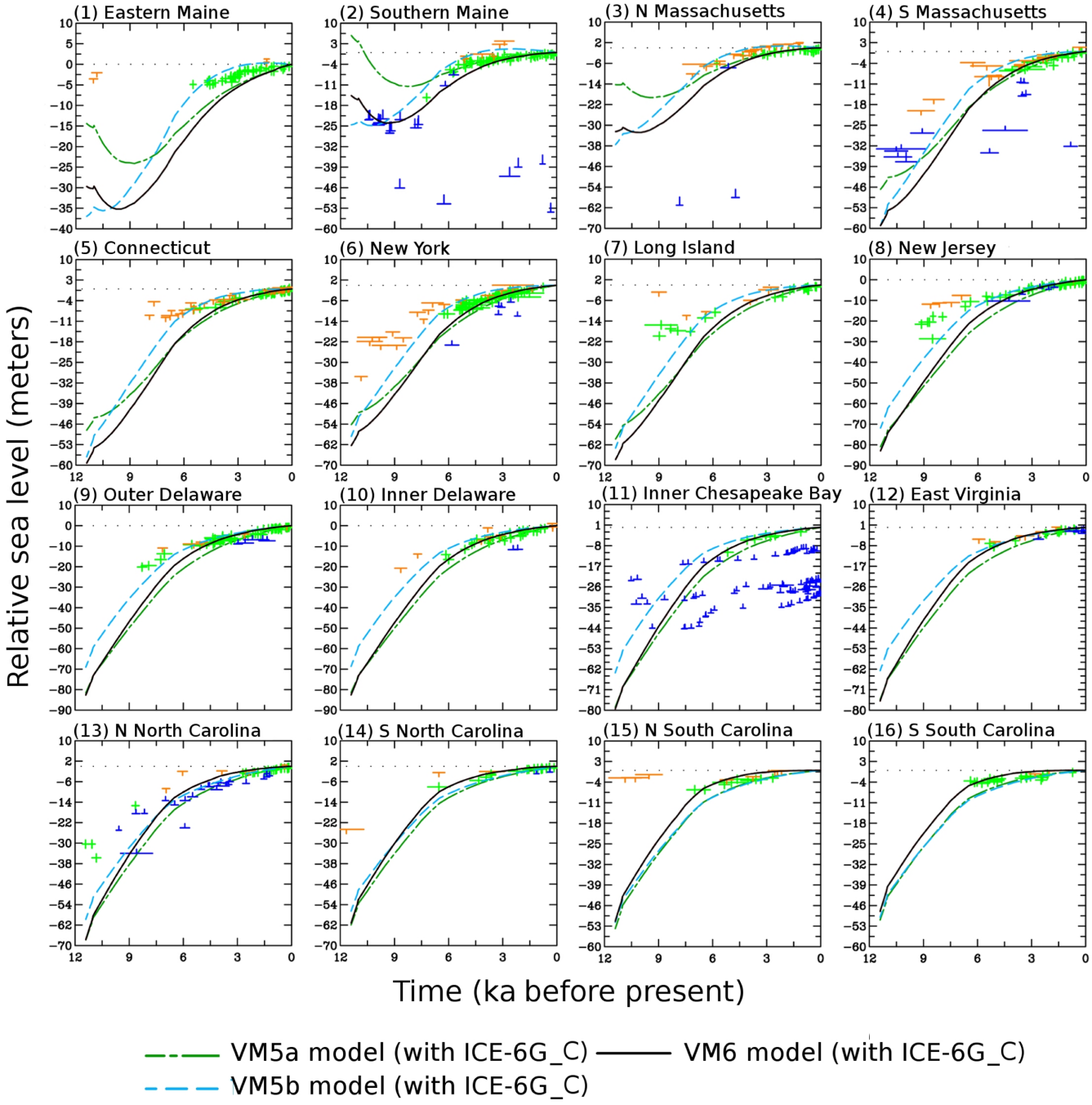

Figure 15. Comparison of the Engelhart *et al.* (2011) data set of relative sea level histories along the U.S. Atlantic coast for the 16 composite regions with the predicted relative sea level history at those locations for the ICE-6G_C model of ice-loading history combined to the VM5a (green), VM5b (blue) and VM6 (black) radial viscosity profiles. Green data points represent sea level index points, whereas blue crosses represent marine-limiting data and orange crosses represent terrestrial-limiting data.

(sites 9–12). In the Carolinas (sites 13–16), particularly in South Carolina, VM6 provides a noted improvement over both VM5a and VM5b. As the misfits associated with the use of these models for the southern part of the Atlantic coast of the United States was an outstanding problem (Engelhart *et al.* 2011), the introduction of this new viscosity structure is important. However, it should be noted that the reduced χ^2 for the Chesapeake Bay region (site 11) and for the northern part of North Carolina (site 13) are strongly impacted by a limited number of relatively old marine-limiting data points, for which some misfits remain.

Another key result is related to the age dependence of the change in χ^2 performance with latitude. As indicated by Table 3, for sites south of Delaware, the increase in performance provided by VM6 is particularly notable for older RSL geological data points (older than 4 ka). In particular, for the southern part of the coast, using the new VM6 viscosity structure removes practically all the misfits with respect to older geological RSL data that were identified when using the VM5a model, with some misfit reductions of more than 95 per cent at some locations. This result is important, as the ability to model older geological data points is crucial if the

Table 3. Percentage change in the reduced χ^2 misfit for the transition from ICE-6G_C (VM5a) to ICE-6G_C (VM6) along the U.S. East coast [negative changes indicate a better fit to the observational data, with −100 per cent representing a complete removal of the misfits observed with ICE-6G_C (VM5a)] (the performance of ICE-6G (VM5b) is also shown for indicative purposes).

Region	Viscosity model transition		
	VM5a → VM5b	VM5a → VM6	
	All RSL data (per cent)	All RSL data (per cent)	Older RSL data (4 ka and older) (per cent)
1- Eastern Maine	–64	70	82
2- Southern Maine	740	250	350
3- North Massachusetts	1075	99	340
4- South Massachusetts	90	360	370
5- Connecticut	190	–33	–55
6- New York	–17	–72	–72
7- Long Island	–75	2.4	2.0
8- New Jersey	–81	–40	–41
9- Outer Delaware	–90	–55	–71
10- Inner Delaware	28	–58	–97
11- Inner Chesapeake Bay	–74	–18	–21
12- East Virginia	–95	–88	–97
13- Northern N. Carolina	–54	–9.2	–23
14- Southern N. Carolina	–50	–2.9	–96
15- Northern S. Carolina	4	–34	–82
16- Southern S. Carolina	43	–45	–94

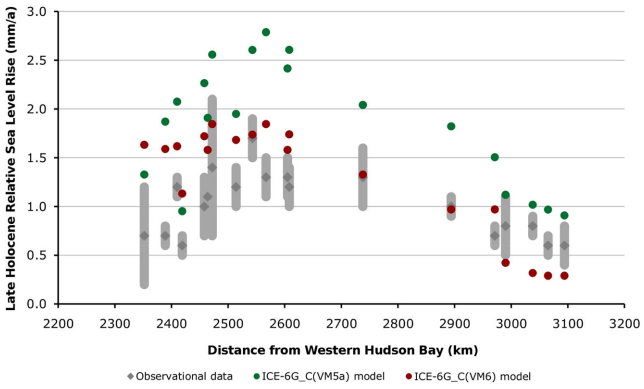

Figure 16. Comparison of observed Late Holocene Relative sea level rise (mm a^{-1}) for locations along U.S. East coast (dark grey diamonds) (with 2σ uncertainty ranges in light grey) (Engelhart *et al.* 2009), with predicted values for the ICE-6G_C (VM5a) (green dots) and ICE-6G_C (VM6) models (red dots). The data points are plotted as a function of distance from the city of Churchill, Manitoba, on the western shore of Hudson Bay (km).

behaviour of the forebulge collapse observed along the U.S. East coast is to be explained correctly, a feature to which we now turn our attention.

Looking in detail at the form of the ongoing collapse of the forebulge predicted to extend over much of the U.S. East coast is an important test of the new VM6 viscosity structure, as the accurate description of the properties of the forebulge is a key component of the study of relative sea level changes observed over the later part of the Holocene and during the 20th century along the U.S. East coast (e.g. Engelhart *et al.* 2009). The shape of the forebulge inferred from the geological records described in Engelhart *et al.* (2011) is presented in Fig. 16 by considering the rates of relative sea level rise over the late Holocene. Following Engelhart *et al.* (2009), these late Holocene rates of relative sea level rise are shown in Fig. 16 for a series of locations along the U.S. East coast as a function of distance from one of the main centres of glaciation of the Laurentide ice sheet (Keewatin dome), approximated to be in modern-day Churchill, Manitoba, on the western shore of Hudson Bay. These values were determined in Engelhart *et al.* (2009) by running a linear regression over the geological data covering the past 4000 yr at each site under consideration (with 2σ error bars). The results obtained for the ICE-6G_C (VM5a) and ICE-6G_C (VM6) models at the same locations are superimposed on Fig. 16.

As shown in Fig. 16, using the VM5a mantle viscosity profile overestimates the late Holocene rates of relative sea level rise for most locations along the U.S. East coast, most notably for locations in the mid-Atlantic states of New Jersey and Delaware (around 2500 km away from the former centre of glaciation), where the most significant forebulge collapse occurs. This results in a forebulge collapse shape (illustrated in Fig. 16 by the slope of uplift rate change as a function of distance from the centre of former glaciation) that compares unfavourably with the geological inference. The VM6 profile captures much better the amplitude of forebulge collapse in most locations, in particular its maximal range, which results in a forebulge collapse shape that is very close to that geologically inferred.

The ability of the ICE-6G_C (VM6) model to capture the geographical extent and the amplitude of forebulge collapse is very significant, since this data was not used in the development of the model. It should also enable an improvement in the characterization of the relative sea level rise observed during the late Holocene and during the 20th century (see Engelhart *et al.* 2009; Kemp *et al.* 2013). Discrepancies remain for the northernmost locations (around Maine), but as these locations are very close to the margin of the former Laurentide ice sheet, these misfits could be eliminated by slight changes in the timing of margin retreat or in the thickness of ice cover in the margin regions. The slight remaining misfit observed in the southernmost locations (around South Carolina) at the trailing edge of the forebulge can be eliminated by a minor change in the stratification of the elastic lithosphere, which will be demonstrated elsewhere.

6.2 Testing the viscosity structure against data from the North American West coast

A further test of the new viscosity structure consists in testing its relative sea level evolution predictions when compared to other observational data sets from other regions relevant to the study of the GIA process. Such a region is the western coast of North America, where a large data set of calibrated ^{14}C-dated sea level indicators has also recently become available (Engelhart *et al.* 2014). The locations of the sites under consideration in this analysis were shown in Fig. 2(b) and span the entire West coast of Canada and of the United States. Since the area is another region undergoing postglacial forebulge collapse, this additional data set will provide an especially important further test of the quality of the new model as the West coast data have not been employed in its development. It is important to note, however, that unlike the Atlantic coast of North America, where the continental margin is relatively 'passive', the Pacific coast is much more active tectonically, as it is notably host in the south to the San Andreas strike slip fault and in the north to the subduction zone that marks the eastern flank of the Juan De Fuca plate. In comparing our results for relative sea level history predictions with the observational constraints, it is important to remain aware that a tectonic overprint is to be expected at some locations. For example, the West coast is known to have been host to the great Cascadia earthquake of 1700 AD (magnitude 8–9; Hawkes *et al.* 2010, 2011), which was undoubtedly accompanied by significant vertical motion. The area is also affected by uplift/subsidence associated with the subduction of the Juan de Fuca plate, especially over Vancouver Island (James *et al.* 2009). However, over the few millennia covered by the data base of existing ^{14}C-dated sea level indicators, this impact should be relatively minor compared to the other uncertainties involved in the study of the GIA problem (viscosity structure of the mantle, ice loading history uncertainty, large spontaneous subsidence/uplift events, impact of sediment compaction on geological records, etc.).

The performance of the VM6 viscosity profile is evaluated along the North American West coast by comparing its RSL history predictions at the sites shown on Fig. 2(b) with the data presented in Fig. 17, starting with the northernmost locations. The model provides a good fit to the available sea level indicators for Queen Charlotte Strait (site 1), as well as the eastern coast of Vancouver Island (site 3). However, on the west coast of Vancouver Island (region 2), a region strongly affected by tectonic impact associated with the subduction of the Juan De Fuca plate, the model not surprisingly fails to reproduce the relative sea level evolution inferred from observational constraints, even though it performs marginally better than VM5a in this regard. For the southeastern part of

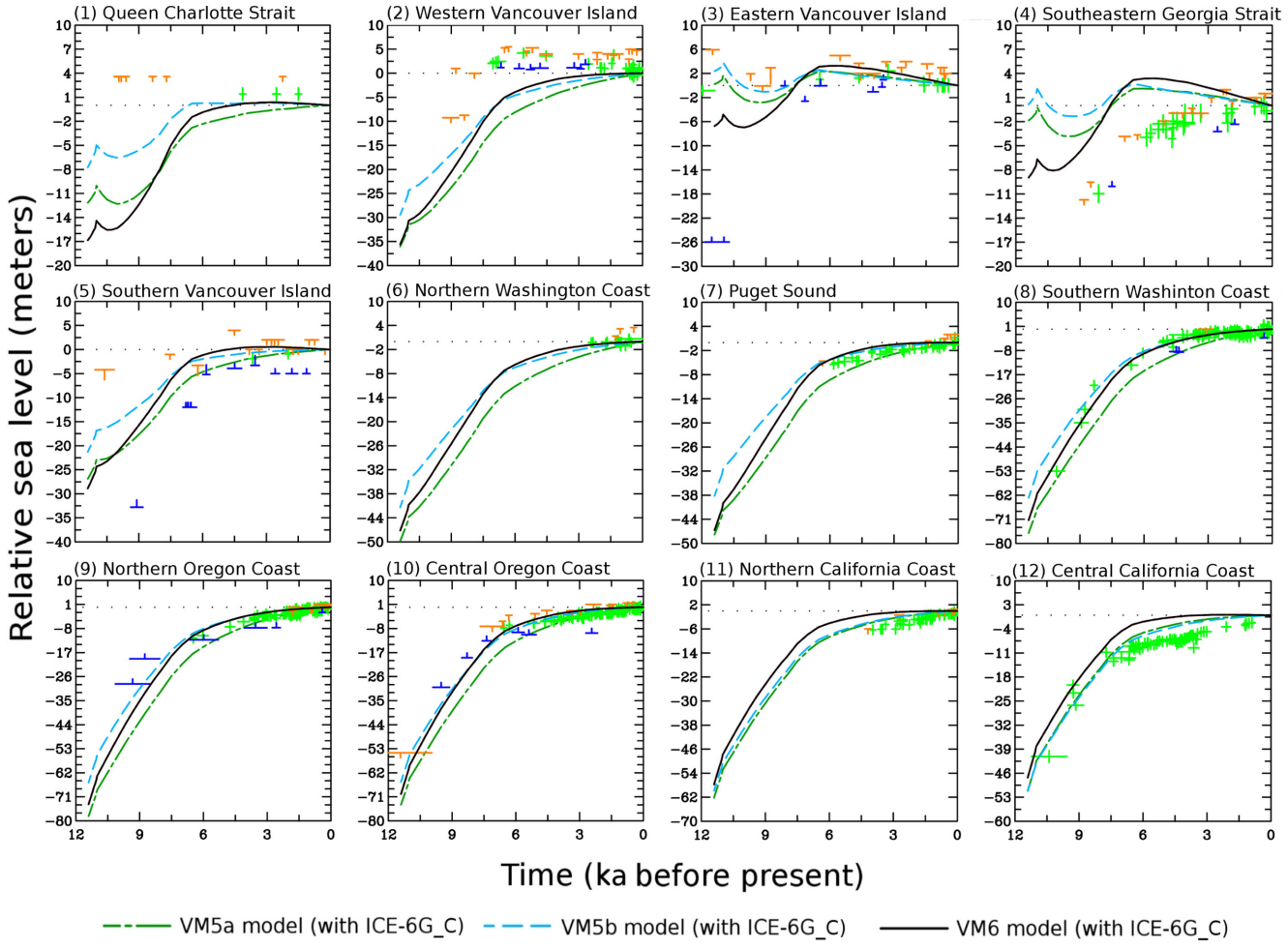

Figure 17. Comparison of a data set of sea level indicators along the North American Pacific coast (Engelhart *et al.* 2014) with the predicted relative sea level history at those locations for the ICE-6G_C model of ice-loading history combined to the VM5a (green), VM5b (blue) and VM6 (black) radial viscosity profiles. Green data points represent sea level index points, whereas blue crosses represent marine-limiting data and orange crosses represent terrestrial-limiting data.

Table 4. Interstudy comparison of secular trends in polar wander and $\dot{J}_2$.

	Source (and data set used, if applicable)	Time covered	Polar motion (° Myr^{-1})	Direction
Polar wander	Argus & Gross (2004) (ILS) (relative to mean lithosphere)	1899–1979	0.98	79.9°W
	Gross & Vondrák (1999) (HIPPARCOS)	1900–1992	0.98	79.2°W
	Gross & Vondrák (1999) (SPACE96)	1976–1997	1.14	73.9°W
	Gross & Poutanen (2009) (SPACE2007)	1976–1995	1.18	72.2°W
	Roy & Peltier (2011) (SPACE2008)	1976–1992	1.25(±0.03)	68(±8)°W
	ICE-6G_C (VM6) prediction	–	1.05	77.6°W
	Source	Time covered	$\dot{J}_2$ ($\times 10^{-11}$ yr^{-1})	
$\dot{J}_2$	Yoder *et al.* (1983)	1978–1983	−3.5	
	Stephenson & Morrison (1995)	700BC–1600AD	−3.5 (±0.8)	
	Cheng & Tapley (2004)	1976–2004	−2.75	
	Roy & Peltier (2011)	1976–1992	−3.7 (±0.1)	
	ICE-6G_C (VM6) prediction	–	−3.36	

Georgia strait (site 4), a region located directly on the mainland, the model fails to predict the subsidence revealed by the geological record for all viscosity structures employed. Instead, it predicts a complex RSL history probably impacted by the rebound associated with the melting of the adjacent Cordilleran ice sheet, the collapse of the forebulge associated with the more remote but much larger Laurentide ice sheet to the east, and the global rise in sea level associated with the last deglaciation. These discrepancies could be explained by various phenomena. In fact, not only is the response in this region heavily impacted by tectonic activity, but the site is also very close to the advancing front of Cordilleran ice during the Last Ice Age and is thus highly sensitive to variations in the ice thickness in its immediate vicinity, most notably in the earlier part of the sea level record. Furthermore, there might be subsidence effects associated with sediment loading caused by glacier meltwater-fed (and thus sediment-rich) water outflows towards Georgia Strait (such as the Fraser and Columbia rivers), which could have impacted certain locations on the eastern shore of Georgia Strait.

For the southern coast of Vancouver Island (site 5), the new VM6 model performs adequately with regards to the limiting data points, although VM5a fits the index points marginally better. However, progressing further south to the Juan de Fuca Strait (site 6) and onwards, the quality of the fit to the observational data improves dramatically. Most notably, along the western coast of Washington State and Oregon, the ICE-6G_C (VM6) model is able to fit very well the observational constraints derived from both sea level index points and terrestrial- or marine-limiting data at all locations. Finally, for the southernmost part of the data set, in California, the models struggle to reproduce the flattening of relative sea level observed between 7.5 and 4 kya. However, it should be noted that the northern part of the Californian coast could be affected by the complex tectonic setting of the region, close to the Mendocino Triple Junction (e.g. Merritts & Bull 1989), while the central coast site, being located within the Sacramento River basin, could also be affected by sediment compaction effects.

6.3 Space-geodetic observations and remaining misfits

Although the new viscosity structure VM6 provides a notably improved fit to the observational data of relative sea evolution on both the East and West coasts of North America, small misfits persist for some locations and time periods. For example, Eastern Maine is a region where a misfit persists, but as mentioned earlier, the issue should not be significant given its location at the margin of the former Laurentide ice sheet. In fact, as relative sea level evolution predictions close to the edges of a former ice sheet are highly dependent on the exact melting history and geometry of the ice sheet, it is expected that these misfits could be removed by modifying the ice loading history near the margins of the former ice sheets. A similar situation applies to the two sites on the eastern shore of Georgia strait on the West coast of the continent. Also, some misfits remain for the U.S. East coast locations situated right at the centre of the forebulge associated with the former Laurentide ice sheet, namely Long Island and New Jersey, regions that could perhaps be affected by compaction issues (Horton *et al.* 2013).

Another set of space-geodetic observations that the new model should be able to fit relates to the rotational state anomalies associated with the continuing impact of the deglaciation that followed LGM. The change in oblateness of figure of the planet (which is related directly to the non-tidal acceleration of the planetary rate of rotation) and true polar wander predicted by the ICE-6G_C (VM6) model may be compared to observations of these anomalies. ICE-6G_C (VM6) model predictions of the evolution of the oblateness of figure are compared to the satellite derived inferences of Yoder *et al.* (1983), Cheng & Tapley (2004) and Roy & Peltier (2011), and to the inference of Stephenson & Morrison (1995) based on the study of historical records of the timing of solar and lunar eclipses. With regards to the true polar wander of the pole of rotation, comparisons to the Earth Orientation Parameter-based values of Gross & Vondrák (1999), Gross & Poutanen (2009) and Roy & Peltier (2011) are provided in Table 4, as well as to the International Latitude Service-based value of Argus & Gross (2004) and Hipparcos-based value of Gross & Vondrák (1999). For the Roy & Peltier (2011) inferences, the comparison to space geodetic inferences focuses on the period 1976–1992, as a modern shift in the secular trend observed in these observables was inferred by these authors to have begun in the early 1990s. The fit of the prediction of the new model to the changing oblateness of figure of the Earth (the time rate of change of the J_2 coefficient of the spherical harmonic expansion of the planetary gravitational field) is excellent. The fit to the true polar wander data is not as good, although the difference between the model prediction and the observations remains small. The good fit provided by ICE-6G_C (VM6) is linked to the increase of the viscosity of the lowermost part of the lower mantle in the transition from VM5a to VM6 (from 3.23×10^{21} to 8.00×10^{21} Pa s). This hardening compensates for the softening of the upper part of the lower mantle necessary in the new VM6 model to fit RSL histories from sites along the southern part of the U.S. East coast. Increasing the value of the viscosity in the lower part of the lower mantle has hardly any effect on RSL predictions along the East coast, as shown explicitly in Fig. 13.

There remains a significant issue that arises when one proceeds in the way we have chosen to employ in the analyses presented herein. Recall that we have elected to keep the loading history fixed to the ICE-6G_C model that is tuned to enable a good fit to a rich data base of GPS observations of vertical motion of the crust as well as to a large number of carbon-dated RSL histories from both Laurentia and Fennoscandia (Peltier *et al.* 2015). Therefore, whether these critical data sets will remain well reconciled by the new ICE-6G_C (VM6) model of the global GIA process remains an important question. If significant misfits to these data were found to exist, then the iterative process we are employing to refine the model might not be convergent. This iterative process consists of alternately fixing the viscosity and the loading history and then refining the other. By returning to investigate the change in the misfits to the available set of GPS observations over the North American continent (e.g. as originally discussed in Argus & Peltier (2010) and Argus *et al.* (2010), and most recently revisited in Peltier *et al.* (2015)) which are effectively eliminated with the ICE-6G_C (VM5a) model, we may close the circle to test convergence. Such a process, using the advocated modifications to the radial profile of mantle viscosity presented herein, will be detailed elsewhere, but initial tests have shown that, with very slight modifications to the ice loading history, the VM6 viscosity profile continues to enable an excellent fit to all of the available GPS vertical crustal movement observations.

7 CONCLUSION AND PERSPECTIVES

The East coast of the continental United States is a very important region in the study of the GIA process. The availability of a new, high-quality data set for all regions along the coast enables the testing of GIA model predictions, most notably concerning models of the radial variation of mantle viscosity. Here, misfits resulting from the use of either the VM5a model (Peltier & Drummond 2008) or the VM5b model (Engelhart *et al.* 2011) have been analysed in detail and shown to be effectively eliminated by the new VM6 model when coupled to the new ICE-6G_C model of global planetary glaciation and deglaciation. Alternative models in the literature (the V1 and V2 models of Mitrovica & Forte 2004 and Forte *et al.* 2009) were also tested and rejected on the basis that the misfits to the data associated with them were found to be even greater than those characteristic of the VM5a and VM5b models.

Through a detailed series of sensitivity tests designed to investigate the response of U.S. East coast RSL histories to variations in the depth dependence of viscosity over specific ranges of mantle depth, we have been led to construct a new model of the radial variation of viscosity in an assumed spherically symmetric model of the Earth's interior. This new model is referred to as VM6, the sixth in the series of models that continue to be refined using the iterative methodology developed to converge upon an optimal structure of this kind. Although the predecessor model VM5a is a perfectly acceptable model insofar as the reconciliation of relative sea level histories and geodetic data from the ice covered regions is concerned, the model fails rather dramatically in the region of forebulge collapse along the U.S. East coast, especially in its southern section. Demonstrating this has required the availability of the new high quality data base that has been assembled in Engelhart *et al.* (2011). The new viscosity model, when combined with the ICE-6G_C loading history, has been shown to eliminate the majority of the misfits that otherwise exist at sites along the U.S. East coast which record the process of forebulge collapse. Independent additional tests of the new model have also been discussed in this paper. The first such independent test involved the analysis of RSL data from the U.S. West coast which is also undergoing the process of glacial forebulge collapse but the data from which were not employed to constrain the new VM6 viscosity structure. With the exception of misfits associated with tectonic influence at a few sites along this coast and with the close proximity of the glacial advance of the Western Cordilleran ice sheet, the new model was shown to reconcile equally well the data from this region as it does along the U.S. East coast. Another independent test of the new model in the North American domain would verify the impact upon the misfit to the voluminous data base of GPS observations of vertical motion of the crust to which the ICE-6G_C (VM5a) model has also been tuned. An analysis of this nature will be presented elsewhere, and it will be shown that the iterative procedure employed to refine the model has effectively separated the errors associated with the loading history from errors associated with the viscosity profile. The misfits that do remain in isolated regions, most notably in the northernmost locations of the U.S. East coast in the data set of Engelhart *et al.* (2011), and in some locations near the crest of the forebulge, are minor compared to those associated with the predictions of the previous ICE-6G_C (VM5a,b) models. These remaining misfits appear to be resilient, in the sense that we have not been able to eliminate them without sacrificing the fit the model provides to the Fennoscandian spectrum of scale-dependent relaxation times. Such persistent misfits could be an indication of lateral heterogeneity in the viscosity structure of the Earth, which is expected to exist based on the nature of the mantle convection process, where upwellings and downwellings are respectively associated with hotter (and less viscous) and colder (and more viscous) material. However, these misfits could also be related to compaction effects in some areas (Horton *et al.* 2013), and will be the subject of further work.

ACKNOWLEDGEMENTS

This sea level research at the University of Toronto has been supported by NSERC Discovery Grant A9627. Further support for the work described in this paper has been provided by NOAA Grant NA11OAR4310101. All computations were performed on the SciNet facility for High Performance Computation which is part of the Compute Canada national HPC platform. We would like to thank Dr David Al-Attar and an anonymous reviewer for their constructive comments on the manuscript. We are indebted to Benjamin Horton, Simon Engelhart, Matteo Vacchi and their colleagues for our continuing interactions regarding their carefully quality-controlled data bases for RSL histories. We are also indebted to Alessandro Forte for sharing with us the viscosity depth dependence data for his V1 and V2 models that we have employed to test their ability to reconcile observations of the GIA process.

REFERENCES

Argus, D.F. & Gross, R.S., 2004. An estimate of motion between the spin axis and the hotspots over the past century, *Geophys. Res. Lett.,* **31,** L06614, doi:10.1029/2004GL019657.

Argus, D.F. & Peltier, W.R., 2010. Constraining models of postglacial rebound using space geodesy: a detailed assessment of model ICE-5G (VM2) and its relatives, *Geophys. J. Int.,* **181**(2), 697–723.

Argus, D.F., Peltier, W.R. & Watkins, M.M., 1999. Glacial isostatic adjustment observed using very long baseline interferometry and satellite laser ranging geodesy, *J. geophys. Res.: Solid Earth,* **104**(B12), 29 077–29 093.

Argus, D.F., Gordon, R.G., Heflin, M.B., Ma, C., Eanes, R.J., Willis, P., Peltier, W.R. & Owen, S.E., 2010. The angular velocities of the plates and the velocity of Earth's centre from space geodesy, *Geophys. J. Int.,* **180**(3), 913–960.

Argus, D.F., Peltier, W.R., Drummond, R. & Moore, A.W., 2014. The Antarctica component of postglacial rebound model ICE-6G_C (VM5a) based on GPS positioning, exposure age dating of ice thicknesses, and relative sea level histories, *Geophys. J. Int.,* **198**(1), 537–563.

Borns, H.W. Jr. *et al.*, 2004. The deglaciation of Maine, U.S.A., in *Quaternary Glaciations—Extent and Chronology, part II,* pp. 89–109, eds Ehlers, J. & Gibbard, P.L., Elsevier.

Cheng, M. & Tapley, B.D., 2004. Variations in the Earth's oblateness during the past 28 years, *J. geophys. Res.: Solid Earth,* **109,** B09402, doi:10.1029/2004JB003028.

Cheng, M., Tapley, B.D. & Ries, J.C., 2013. Deceleration in the Earth's oblateness, *J. geophys. Res.: Solid Earth,* **118**(2), 740–747.

Clark, J.A., Farrell, W.E. & Peltier, W.R., 1978. Global changes in postglacial sea level—numerical calculation, *Quatern. Res.,* **9**(3), 265–287.

Donner, J., 1995. *The Quaternary History of Scandinavia, World and Regional Geology Series,* Vol. 7, Cambridge Univ. Press.

Dyke, A.S., 2004. An outline of North American deglaciation with emphasis on central and northern Canada, in *Quaternary Glaciations—Extent and Chronology, Part II,* pp. 373–424, eds Ehlers, J. & Gibbard, P.L., Elsevier.

Dyke, A.S. & Peltier, W.R., 2000. Forms, response times and variability of relative sea-level curves, glaciated North America, *Geomorphology,* **32**(3–4), 315–333.

Dyke, A.S., Andrews, J.T., Clark, P.U., England, J.H., Miller, G.H., Shaw, J. & Veillette, J.J., 2002. The Laurentide and Innuitian ice sheets during the Last Glacial Maximum, *Quarter. Sci. Rev.,* **21**(1–3), 9–31.

Engelhart, S.E., Horton, B.P., Douglas, B.C., Peltier, W.R. & Törnqvist, T.E., 2009. Spatial variability of late Holocene and 20th century sea-level rise along the Atlantic coast of the United States, *Geology,* **37**(12), 1115–1118.

Engelhart, S.E., Peltier, W.R. & Horton, B.P., 2011. Holocene relative sea-level changes and glacial isostatic adjustment of the US Atlantic coast, *Geology,* **39**(8), 751–754.

Engelhart, S.E., Vacchi, M., Horton, B.P., Nelson, A.R. & Kopp, R.E., 2014. A sea-level database for the Pacific coast of central North America, *Quatern. Sci. Rev.,* in press.

Fairbanks, R.G., 1989. A 17,000-year glacio-eustatic sea-level record—influence of glacial melting rates on the Younger Dryas event and deep-ocean circulation, *Nature,* **342**(6250), 637–642.

Farrell, W.E., 1972. Deformation of Earth by surface loads, *Rev. Geophys. Space Phys.,* **10**(3), 761–797.

Farrell, W.E. & Clark, J.A., 1976. Postglacial sea level, *Geophys. J. R. astr. Soc.,* **46**(3), 647–667.

Forte, A.M. & Mitrovica, J.X., 1996. New inferences of mantle viscosity from joint inversion of long-wavelength mantle convection and post-glacial rebound data, *Geophys. Res. Lett.,* **23**(10), 1147–1150.

Forte, A.M. & Mitrovica, J.X., 1997. Radial profile of mantle viscosity: results from the joint inversion of convection and postglacial rebound observables, *J. geophys. Res.,* **102**(B2), 2751–2769.

Forte, A.M., Moucha, R., Rowley, D.B., Quéré, S., Mitrovica, J.X., Simmons, N.A. & Grand, S.P., 2009. Recent tectonic plate decelerations driven by mantle convection, *Geophys. Res. Lett.,* **36,** L23301, doi:10.1029/2009GL040224.

Forte, A.M., Peltier, W.R. & Dziewonski, A.M., 1991. Inferences of mantle viscosity from tectonic plate velocities, *Geophys. Res. Lett.,* **18**(9), 1747–1750.

Forte, A.M., Peltier, W.R., Dziewonski, A.M. & Woodward, R.L., 1993. Dynamic surface-topography—a new interpretation based upon mantle flow models derived from seismic tomography, *Geophys. Res. Lett.,* **20**(3), 225–228.

Gross, R.S. & Poutanen, M., 2009. Geodectic observations of glacial isostatic adjustment, *EOS, Trans. Am. geophys. Un.,* **90**(41), 365, doi:10.1029/2009EO410004.

Gross, R.S. & Vondrák, J., 1999. Astrometric and space-geodetic observations of polar wander, *Geophys. Res. Lett.,* **26**(14), 2085–2088.

Hawkes, A.D., Horton, B.P., Nelson, A.R. & Hill, D.F., 2010. The application of intertidal foraminifera to reconstruct coastal subsidence during the giant Cascadia earthquake of AD 1700 in Oregon, *Quatern. Int.,* **221,** 116–140.

Hawkes, A.D., Horton, B.P., Nelson, A.R., Vane, C.H. & Sawai, Y., 2011. Coastal subsidence in Oregon, USA, during the giant Cascadia earthquake of AD 1700, *Quatern. Sci. Rev.,* **30,** 364–376.

Horton, B.P., Engelhart, S.E., Hill, D.F., Kemp, A.C., Nikitina, D., Miller, K.G. & Peltier, W.R., 2013. Influence of tidal-range change and sediment compaction on Holocene relative sea-level change in New Jersey, USA, *J. Quarter. Sci.,* **28**(4), 403–411.

Ivins, E.R., James, T.S., Wahr, J., Schrama, E.J.O., Landerer, F.W. & Simon, K.M., 2013. Antarctic contribution to sea level rise observed by GRACE with improved GIA correction, *J. geophys. Res.: Solid Earth,* **118**(6), 3126–3141.

James, T.S., Gowan, E.J., Hutchinson, I., Clague, J.J., Barrie, J.V. & Conway, K.W., 2009. Sea-level change and paleogeographic reconstructions for southern Vancouver Island, British Columbia, Canada, *Quatern. Sci. Rev.,* **28**(13–14), 1200–1216.

Kemp, A.C. *et al.*, 2013. Sea-level change during the last 2500 years in New Jersey, USA, *Quatern. Sci. Rev.,* **81,** 90–104.

Luthcke, S.B., Sabaka, T.J., Loomis, B.D., Arendt, A.A., McCarthy, J.J. & Camp, J., 2013. Antarctica, Greenland and Gulf of Alaska land-ice evolution from an iterated GRACE global mascon solution, *J. Glaciol.,* **59**(216), 613–631.

McConnell, R.K., 1968. Viscosity of the mantle from relaxation time spectra of isostatic adjustment, *J. Geophys. Res.,* **73**(22), 7089–7105.

Merritts, D. & Bull, W.B., 1989. Interpreting Quaternary uplift rates at the Mendocino triple junction, northern California, from uplifted marine terraces, *Geology,* **17,** 1020–1024.

Miousse, L., Bhiry, N. & Lavoie, M., 2003. Isolation and water-level fluctuations of Lake Kachishayoot, Northern Québec, Canada, *Quatern. Res.,* **60,** 149–161.

Mitrovica, J.X. & Forte, A.M., 2004. A new inference of mantle viscosity based upon joint inversion of convection and glacial isostatic adjustment data, *Earth planet. Sci. Lett.,* **225**(1–2), 177–189.

Mitrovica, J.X. & Peltier, W.R., 1991. A complete formalism for the inversion of postglacial rebound data—resolving power analysis, *Geophys. J. Int.,* **104**(2), 267–288.

Mitrovica, J.X. & Peltier, W.R., 1993. The inference of mantle viscosity from an inversion of the Fennoscandian relaxation spectrum, *Geophys. J. Int.,* **114**(1), 45–62.

Mitrovica, J.X. & Peltier, W.R., 1995. Constraints on mantle viscosity based upon the inversion of postglacial uplift data from the Hudson Bay region, *Geophys. J. Int.,* **122**(2), 353–377.

Mitrovica, J.X., Forte, A.M. & Simons, M., 2000. A reappraisal of postglacial decay times from Richmond Gulf and James Bay, Canada, *Geophys. J. Int.,* **142**(3), 783–800.

Moucha, R., Forte, A.M., Mitrovica, J.X., Rowley, D.B., Quéré, S., Simmons, N.A. & Grand, S.P., 2008. Dynamic topography and long-term sea-level variations: there is no such thing as a stable continental platform, *Earth planet. Sci. Lett.,* **271**(1–4), 101–108.

Pari, G. & Peltier, W.R., 1995. The heat-flow constraint on mantle tomography-based convection models—towards a geodynamically self-consistent inference of mantle viscosity, *J. geophys. Res.: Solid Earth,* **100**(B7), 12 731–12 751.

Pari, G. & Peltier, W.R., 1996. The free-air gravity constraint on subcontinental mantle dynamics, *J. geophys. Res.: Solid Earth,* **101**(B12), 28 105–28 132.

Pari, G. & Peltier, W.R., 2000. Subcontinental mantle dynamics: a further analysis based on the joint constraints of dynamic surface topography and free-air gravity, *J. geophys. Res.: Solid Earth,* **105**(B3), doi:10.1029/1999JB900349.

Pearson, D.G. *et al.*, 2014. Hydrous mantle transition zone indicated by ringwoodite included within diamond, *Nature,* **507,** 221–224.

Peltier, W.R., 1974. Impulse response of a Maxwell Earth, *Rev. Geophys.,* **12**(4), 649–669.

Peltier, W.R., 1976. Glacial isostatic adjustment: II—Inverse problem, *Geophys. J. R. astr. Soc.,* **46**(3), 669–705.

Peltier, W.R., 1982. Dynamics of the ice-age Earth, *Adv. Geophys.,* **24,** 1–142.

Peltier, W.R., 1985. The LAGEOS constraint on deep mantle viscosity—results from a new normal mode method for the inversion of viscoelastic relaxation, *J. geophys. Res.: Solid Earth Planets,* **90**(NB11), 9411–9421.

Peltier, W.R., 1989. Mantle viscosity, in *Mantle Convection,* pp. 389–478, ed. Peltier, W.R., Gordon and Breach.

Peltier, W.R., 1994. Ice-age paleotopography, *Science,* **265**(5169), 195–201.

Peltier, W.R., 1996a. Mantle viscosity and ice-age ice sheet topography, *Science,* **273**(5280), 1359–1364.

Peltier, W.R., 1996b. Global sea level rise and glacial isostatic adjustment: an analysis of data from the East Coast of North America, *Geophys. Res. Lett.,* **23**(7), 717–720.

Peltier, W.R., 1998a. A space geodetic target for mantle viscosity determination: horizontal motions induced by glacial isostatic adjustment, *Geophys. Res. Lett.,* **25**(4), 543–546.

Peltier, W.R., 1998b. The inverse problem for mantle viscosity, *Inverse Probl.,* **14**(3), 441–478.

Peltier, W.R., 1998c. Postglacial variations in the level of the sea: implications for climate dynamics and solid-Earth geophysics, *Rev. Geophys.,* **36**(4), 603–689.

Peltier, W.R., 1998d. "Implicit ice" in the global theory of glacial isostatic adjustment, *Geophys. Res. Lett.,* **25**(21), 3955–3958.

Peltier, W.R., 2002. On eustatic sea level history: Last Glacial Maximum to Holocene, *Quatern. Sci. Rev.,* **21**(1–3), 377–396.

Peltier, W.R., 2004. Global glacial isostasy and the surface of the ice-age Earth: the ICE-5G (VM2) model and GRACE, *Annu. Rev. Earth Pl. Sc.,* **32,** 111–149.

Peltier, W.R., 2007. History of Earth rotation, in *Treatise of Geophysics,* Vol. 9, pp. 243–293, ed. Schubert, G., Elsevier Press.

Peltier, W.R., 2009. Closure of the budget of global sea level rise over the GRACE era: the importance and magnitudes of the required corrections for global glacial isostatic adjustment, *Quatern. Sci. Rev.,* **28**(17–18), 1658–1674.

Peltier, W.R. & Andrews, J.T., 1976. Glacial isostatic adjustment: I—Forward problem, *Geophys. J. R. astr. Soc.,* **46**(3), 605–646.

Peltier, W.R. & Drummond, R., 2008. Rheological stratification of the lithosphere: a direct inference based upon the geodetically observed pattern of the glacial isostatic adjustment of the North American continent, *Geophys. Res. Lett.,* **35**(16), L16314, doi:10.1029/2008GL034586.

Peltier, W.R. & Fairbanks, R.G., 2006. Global glacial ice volume and Last Glacial Maximum duration from an extended Barbados sea level record, *Quatern. Sci. Rev.,* **25**(23–24), 3322–3337.

Peltier, W.R. & Jiang, X.H., 1996. Mantle viscosity from the simultaneous inversion of multiple data sets pertaining to postglacial rebound, *Geophys. Res. Lett.,* **23**(5), 503–506.

Peltier, W.R. & Luthcke, S.B., 2009. On the origins of Earth rotation anomalies: new insights on the basis of both "paleogeodetic" data and Gravity Recovery and Climate Experiment (GRACE) data, *J. geophys. Res.: Solid Earth,* **114,** B11405, doi:10.1029/2009JB006352.

Peltier, W.R. & Tushingham, A.M., 1989. Global sea level rise and the greenhouse effect: might they be connected?, *Science,* **244**(4906), 806–810.

Peltier, W.R. & Vettoretti, G., 2014. Dansgaard-Oeschger oscillations predicted in a comprehensive model of glacial climate: a "kicked" salt oscillator in the Atlantic, *Geophys. Res. Lett.,* **41**(20), 7303–7306.

Peltier, W.R., Farrell, W.E. & Clark, J.A., 1978. Glacial isostasy and relative sea level—global finite-element model, *Tectonophysics,* **50**(2–3), 81–110.

Peltier, W.R., Drummond, R. & Tushingham, A.M., 1986. Postglacial rebound and transient lower mantle rheology, *Geophys. J. R. astr. Soc.,* **87**(1), 79–116.

Peltier, W.R., Shennan, I., Drummond, R. & Horton, B.P., 2002. On the postglacial isostatic adjustment of the British Isles and the shallow viscoelastic structure of the Earth, *Geophys. J. Int.,* **148**(3), 443–475.

Peltier, W.R., Drummond, R. & Roy, K., 2012. Comment on "Ocean mass from GRACE and glacial isostatic adjustment" by D.P. Chambers *et al.*, *J. geophys. Res.: Solid Earth,* **117,** B11403, doi:10.1029/2011JB008967.

Peltier, W.R., Argus, D.F. & Drummond, R., 2015. Space geodesy constrains ice-age terminal deglaciation: the global ICE-6G_C (VM5a) model, *J. geophys. Res.: Solid Earth,* **119,** doi:10.1002/2014JB011176.

Pendea, I.F., Costopoulos, A., Nielsen, C. & Chmura, G.L., 2010. A new shoreline displacement model for the last 7 ka from eastern James Bay, Canada, *Quatern. Res.,* **73**(3), 474–484.

Ratcliff, J.T. & Gross, R.S., 2013. *Combinations of Earth Orientation Measurements: SPACE2012, COMB2012, and POLE2012,* JPL Publication 13–16, Jet Propul. Lab.

Roy, K. & Peltier, W.R., 2011. GRACE era secular trends in Earth rotational parameters: a global scale impact of the global warming process?, *Geophys. Res. Lett.,* **38,** L10306, doi:10.1029/2011GL047282.

Saulnier-Talbot, É. & Pienitz, R., 2001. Isolation au post-glaciaire d'un bassin côtier près de Kuujjuaraapik-Whapmagoostui, en Hudsonie (Québec): une analyse biostratigraphique diatomifère, *Geogr. Phys. Quatern.,* **55,** 63–74.

Sella, G.F., Stein, S., Dixon, T.H., Craymer, M., James, T.S., Mazzotti, S. & Dokka, R.K., 2007. Observation of glacial isostatic adjustment in "stable" North America with GPS, *Geophys. Res. Lett.,* **34**(2), L02306, doi:10.1029/2006GL027081.

Shennan, I., Innes, J.B., Long, A.J. & Zong, Y.Q., 1994. Late Devensian and Holocene relative sea-level changes at Loch-Nan-Eala, near Arisaig, Northwest Scotland, *J. Quarter. Sci.,* **9**(3), 261–283.

Shennan, I., Peltier, W.R., Drummond, R. & Horton, B., 2002. Global to local scale parameters determining relative sea-level changes and the post-glacial isostatic adjustment of Great Britain, *Quater. Sci. Rev.,* **21**(1–3), 397–408.

Steffen, H. & Wu, P., 2011. Glacial isostatic adjustment in Fennoscandia—a review of data and modelling, *J. Geodyn.,* **52**(3–4), 169–204.

Stephenson, E.R. & Morrison, L.V., 1995. Long term fluctuations in the Earth's rotation: 700 B.C. to A.D., 1990, *Phil. Trans. R. Soc. Lond., A,* **351,** 165–202.

Tushingham, A.M. & Peltier, W.R., 1991. ICE-3G—a new global model of late Pleistocene deglaciation based upon geophysical predictions of postglacial relative sea-level change, *J. geophys. Res.: Solid Earth Planets,* **96**(B3), 4497–4523.

Tushingham, A.M. & Peltier, W.R., 1992. Validation of the ICE-3G model of Wurm-Wisconsin deglaciation using a global data-base of relative sea-level histories, *J. geophys. Res.: Solid Earth.,* **97**(B3), 3285–3304.

van de Plassche, O., 1986. *Sea-Level Research: A Manual for the Collection and Evaluation of Data,* 1st edn, Geobooks, 618 pp.

Velicogna, I. & Wahr, J., 2013. Time-variable gravity observations of ice sheet mass balance: precision and limitations of the GRACE satellite data, *Geophys. Res. Lett.,* **40**(12), 3055–3063.

Vettoretti, G. & Peltier, W.R., 2013. Last Glacial Maximum ice sheet impacts on North American climate variability: the importance of the sea ice lid, *Geophys. Res. Lett.,* **40**(24), 6378–6383.

Whitehouse, P.L., Bentley, M.J. & Le Brocq, A.M., 2012. A deglacial model for Antarctica: geological constraints and glaciological modelling as a basis for a new model of Antarctic glacial isostatic adjustment, *Quat. Sci. Rev.,* **32,** 1–24.

Wieczerkowski, K., Mitrovica, J.X. & Wolf, D., 1999. A revised relaxation-time spectrum for Fennoscandia, *Geophys. J. Int.,* **139**(1), 69–86.

Wu, P. & Peltier, W.R., 1983. Glacial isostatic adjustment and the free air gravity anomaly as a constraint on deep mantle viscosity, *Geophys. J. R. astr. Soc.,* **74**(2), 377–449.

Wu, P. & Peltier, W.R., 1984. Pleistocene deglaciation and the Earth's rotation: a new analysis, *Geophys. J. R. astr. Soc.,* **76**(3), 753–791.

Wu, P., Steffen, H. & Wang, H., 2010. Optimal locations for GPS measurements in North America and northern Europe for constraining Glacial Isostatic Adjustment, *Geophys. J. Int.,* **181**(2), 653–664.

Yoder, C.F., Williams, J.G., Dickey, J.O., Schutz, B.E., Eanes, R.J. & Tapley, B.D., 1983. Secular variation of the Earth's gravitational harmonic J_2 coefficient from LAGEOS and non-tidal acceleration of Earth rotation, *Nature,* **303,** 757–762.

SUPPORTING INFORMATION

Additional Supporting Information may be found in the online version of this paper:

Figure S1. Comparison of all 16 regions of the Engelhart *et al.* (2011) data set of relative sea level histories along the U.S. Atlantic coast with the predicted relative sea level history at those locations for the ICE-6G_C model of ice-loading history combined to the V1 (green) and V2 (blue) radial viscosity profiles. The results for the VM5a (black) and VM5b (red) models are shown for comparison. Green data points represent sea level index points, whereas blue crosses represent marine-limiting data and orange crosses represent terrestrial-limiting data.

Figure S2. Comparison of all 16 regions of the Engelhart *et al.* (2011) data set of relative sea level histories along the U.S. Atlantic coast with the predicted relative sea level history at those locations for the ICE-6G_C model of ice-loading history combined to viscosity profiles where the viscosity of the upper mantle (UM) is allowed to vary (as discussed in the text). Green data points represent sea level index points, whereas blue crosses represent marine-limiting data and orange crosses represent terrestrial-limiting data.

Figure S3. Comparison of all 16 regions of the Engelhart *et al.* (2011) data set of relative sea level histories along the U.S. Atlantic coast with the predicted relative sea level history at those locations for the ICE-6G_C model of ice-loading history combined to viscosity profiles where the viscosity of the upper part of the lower mantle (ULM) is allowed to vary (as discussed in the text). Green data points represent sea level index points, whereas blue crosses represent marine-limiting data and orange crosses represent terrestrial-limiting data.

Figure S4. Comparison of all 16 regions of the Engelhart *et al.* (2011) data set of relative sea level histories along the U.S. Atlantic coast with the predicted relative sea level history at those locations for the ICE-6G_C model of ice-loading history combined to viscosity profiles where the viscosity of the transition zone (TZ) is allowed to vary (as discussed in the text). Green data points represent sea level index points, whereas blue crosses represent marine-limiting data and orange crosses represent terrestrial-limiting data.

Figure S5. Comparison of all 16 regions of the Engelhart *et al.* (2011) data set of relative sea level histories along the U.S. Atlantic coast with the predicted relative sea level history at those locations for the ICE-6G_C model of ice-loading history combined to viscosity profiles where the viscosity contrast between the upper and lower mantles is allowed to vary (as discussed in the text). Green data points represent sea level index points, whereas blue crosses represent marine-limiting data and orange crosses represent terrestrial-limiting data.

Figure S6. Comparison of all 16 regions of the Engelhart *et al.* (2011) data set of relative sea level histories along the U.S. Atlantic coast with the predicted relative sea level history at those locations for the ICE-6G_C model of ice-loading history combined to viscosity profiles where the thickness of the elastic lithosphere is allowed to vary (as discussed in the text). Green data points represent sea level index points, whereas blue crosses represent marine-limiting data and orange crosses represent terrestrial-limiting data.

Figure S7. Comparison of a subset of regions of the Engelhart *et al.* (2011) data set of relative sea level histories along the U.S. Atlantic coast with the predicted relative sea level history at those locations for the ICE-6G_C model of ice-loading history combined to viscosity profiles where the viscosity of the lower part of the lower mantle is allowed to vary (as discussed in the text). Green data points represent sea level index points, whereas blue crosses represent marine-limiting data and orange crosses represent terrestrial-limiting data.

Table S1. Detailed reduced χ^2 comparison for mantle viscosity variation cases considered. (http://gji.oxfordjournals.org/lookup/suppl/doi:10.1093/gji/ggv066/-/DC1)

Please note: Oxford University Press is not responsible for the content or functionality of any supporting materials supplied by the authors. Any queries (other than missing material) should be directed to the corresponding author for the paper.